Chemical Research in Toxicology

Article

Cite This: Chem. Res. Toxicol. 2019, 32, 2382−2397

pubs.acs.org/crt

Iron Oxide Nanoparticle-Induced Neoplastic-Like Cell Transformation *in Vitro* Is Reduced with a Protective Amorphous Silica Coating

Tiffany G. Kornberg,*[,†,§] Todd A. Stueckle,[§] Jayme Coyle,[§] Raymond Derk,[§] Philip Demokritou,[∥] Yon Rojanasakul,[†] and Liying W. Rojanasakul*[,†,§]

[†]Department of Pharmaceutical and Pharmacological Sciences, School of Pharmacy, West Virginia University, Morgantown, West Virginia 26506, United States

[§]Allergy and Clinical Immunology Branch, Health Effects Laboratory Division, National Institute for Occupational Safety and Health, Morgantown, West Virginia 26505, United States

[∥]Center for Nanotechnology and Nanotoxicology, Department of Environmental Health, T.H. Chan School of Public Health, Harvard University, Boston, Massachusetts 02115, United States

Supporting Information

ABSTRACT: Iron oxide nanoparticles (IONP) have recently surged in production and use in a wide variety of biomedical and environmental applications. However, their potential long-term health effects, including carcinogenesis, are unknown. Limited research suggests IONP can induce genotoxicity and neoplastic transformation associated with particle dissolution and release of free iron ions. "Safe by design" strategies involve the modification of particle physicochemical properties to affect subsequent adverse outcomes, such as an amorphous silica coating to reduce IONP dissolution and direct interaction with cells. We hypothesized that long-term exposure to a specific IONP (nFe_2O_3) would induce neoplastic-like cell transformation, which could be prevented with an amorphous silica coating (SiO_2-nFe_2O_3). To test this hypothesis, human bronchial epithelial cells (Beas-2B) were continuously exposed to a 0.6 $\mu g/cm^2$ administered a dose of nFe_2O_3 (~0.58 $\mu g/cm^2$ delivered dose), SiO_2-nFe_2O_3 (~0.55 $\mu g/cm^2$ delivered dose), or gas metal arc mild steel welding fumes (GMA-MS, ~0.58 $\mu g/cm^2$ delivered dose) for 6.5 months. GMA-MS are composed of roughly 80% iron/iron oxide and were recently classified as a total human carcinogen. Our results showed that low-dose/long-term *in vitro* exposure to nFe_2O_3 induced a time-dependent neoplastic-like cell transformation, as indicated by increased cell proliferation and attachment-independent colony formation, which closely matched that induced by GMA-MS. This transformation was associated with decreases in intracellular iron, minimal changes in reactive oxygen species (ROS) production, and the induction of double-stranded DNA damage. An amorphous silica-coated but otherwise identical particle (SiO_2-nFe_2O_3) did not induce this neoplastic-like phenotype or changes in the parameters mentioned above. Overall, the presented data suggest the carcinogenic potential of long-term nFe_2O_3 exposure and the utility of an amorphous silica coating in a "safe by design" hazard reduction strategy, within the context of a physiologically relevant exposure scenario (low-dose/long-term), with model validation using GMA-MS.

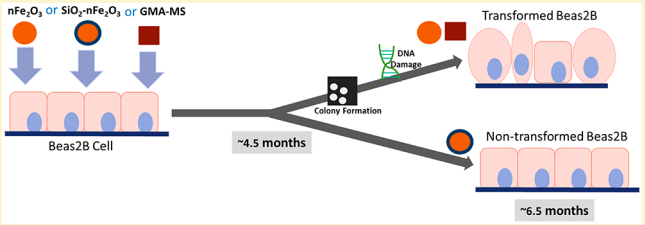

INTRODUCTION

Nanosized materials, which are specifically engineered to be 100 nm or smaller in at least one dimension, have emerged as novel solutions to critical issues in areas such as medicine, biotechnology, and transportation. Of these, iron oxide nanoparticles (IONP) have been investigated as unique components of MRI imaging techniques,[1] targeted drug delivery systems,[2] environmental catalysts,[3] and incorporation into thermoplastics,[4,5] food products,[6] and toners for printing equipment.[7] IONP, as well as many other types of nanometal oxides, have also grown in interest, production, and utilization for consumer products, including agriculture and food applications.[8−10] This surge may translate to an increased risk of exposure for those involved in particle manufacture and use across its life cycle. However, potentially adverse health outcomes following extended periods of exposure to IONP remain unclear.

One of the most common routes for human exposure is the inhalation of particulates in the circulating air, which usually occurs at low doses over long periods of time. This type of exposure can have distinct adverse outcomes for vulnerable populations. Chronic pulmonary exposure to metal-oxide particulates has been associated with cancer development in miners, welders, and other types of industrial workers.[11] However, potential cancer-related outcomes induced by IONP,

Received: March 18, 2019
Published: October 28, 2019

DOI: 10.1021/acs.chemrestox.9b00118
Chem. Res. Toxicol. 2019, 32, 2382−2397

as well as other types of nanometal oxides, remain poorly understood. For IONP, the current standard is to regulate exposure based on fine-sized (100−2500 nm[12]) iron oxide exposure limits, even though evidence suggests that nanosized particulates may pose a greater risk with exposure on a per mass basis than their fine-sized counterparts.[13,14]

As a further complication, fine-sized iron oxide has an unclear and controversial toxicity profile. Some researchers suggest this particulate is essentially benign,[15−20] whereas others associate exposure with adverse pulmonary outcomes, including increased risk of lung cancer in iron ore miners.[21−23] Similarly, IONP-induced adverse health outcomes are also largely unclear. It is known there is some risk of occupational exposure to IONP,[24,25] with unknown or unreported adverse outcomes. In laboratory settings, some researchers report no effect following IONP exposure,[26−28] whereas others indicate that IONP or IONP-containing materials may induce genotoxicity,[29−32] neoplastic-like cell transformation,[33,34] *in vivo* tumor formation,[35,36] and neurotoxicity.[37]

Gas metal arc welding fumes (GMA) have recently been reclassified as a Group 1 total human carcinogen.[38] GMA generated from mild steel welding (GMA-MS) contains roughly 80% of iron/iron oxide particulates that fall within the nanosize range. GMA-MS exposure is associated with fibrotic lesions and elevated lung iron levels in humans,[39] as well as lung tumor development[35,36] and lung cancer progression.[40] Although GMA-MS contains largely insoluble iron, it still provides a useful reference for potential IONP-induced adverse outcomes, particularly those related to the induction or promotion of lung cancer.

The aims of this study were to assess the potential for IONP to induce neoplastic-like cell transformation within the context of an occupationally relevant subchronic *in vitro* exposure model (low-dose/long-term) and to examine the potential protective qualities of an amorphous silica coating under these conditions. GMA-MS particles were used as a positive control, as they have been previously shown to promote carcinogenic outcomes *in vivo*.[35,36] Particle-induced changes in intracellular iron, ROS production, and DNA damage associated with the cell transformation were also evaluated throughout the long-term exposure.

EXPERIMENTAL METHODS

Particle Generation, Preparation, Characterization, and Dosimetry. nFe_2O_3, SiO_2-nFe_2O_3, and SiO_2 were generated at Harvard University Center for Nanotechnology and Nanotoxicology (Boston, MA) using the VEGNES-FSP system.[41] Briefly, this flame spray pyrolysis synthesis platform involves the dispersion of organometallic precursors (iron) and their combustion to form nFe_2O_3. Immediately following combustion, particles were sprayed with SiO_2 vapor to form a nanothin amorphous silica coating,[41,42] before collection on Teflon filters. Particles were then extracted as powders for subsequent experiments. Gas metal arc mild steel welding fumes (GMA-MS) were generated at the Lincoln Electric Co. (St. Louis, MO) and provided by Dr. James M. Antonini from CDC/NIOSH (Morgantown, WV). These fumes were generated in a fume chamber by a skilled welder, and particulates were collected on filters for use in this study.[43] Aeroxide TiO_2 (80:20 anatase/rutile structure, Evonik) was supplied from the Degussa Corporation (Parsippany, NJ) and provided by Dr. Tina Sager from CDC/NIOSH (Morgantown, WV).[44] TiO_2 particulates were sieved at a vibration amplitude of 50 and then filtered three times using Teflon filters (1.18 mm, 250 nm, and 45 nm). Only particles that were able to pass through all three filters were used for treatments. TiO_2 was used as a reference particle control, as the same particle is the source material for NIST Standard Reference Material for TiO_2.[45]

Partial particle characterization in the pristine powder phase was previously determined as described for nFe_2O_3, SiO_2-nFe_2O_3, and SiO_2 (d_{XRD}, SSA, and iron/iron oxide content),[41] TiO_2 (d_{XRD}),[44] and GMA-MS (iron/iron oxide content).[43] The d_{XRD} of GMA-MS was calculated based on representative SEM images. Particles were suspended in sterilized Milli-Q water at a concentration of 1 mg/mL in sterilized glass test tubes. Particle suspensions were sonicated with a cup horn sonicator (Sonics Vibra Cell, Newton, CT) based on sonicator efficiency and calculated critical energy needed to generate stable particle agglomerates (nFe_2O_3/SiO_2-nFe_2O_3, 242 J/mL; SiO_2, 161 J/mL; TiO_2, 161 J/mL; GMA-MS, 242 J/mL)[46−48] and were then serially diluted in BEGM for subsequent treatment. Fresh particle stock suspensions in water were prepared every 4 weeks and sonicated a maximum of eight consecutive times in water, with a hydrodynamic diameter (d_H) in medium determined separately for each sonication.

Hydrodynamic diameter (d_H) and ζ potential for all particles following suspension in Milli-Q water, sonication, and serial dilution in a complete cell culture medium were determined by dynamic light scattering (DLS, ZetaSizer Nano ZS, Model Zen3600, Malvern, Surrey, United Kingdom) using previously described methods.[47,48] The ζ potential was determined using the ZetaSizer Nano Series Dip Cell (Model Zen1002, Malvern, Surrkey, United Kingdom). For scanning electron microscopy (SEM) with energy-dispersive X-ray (EDX), particles in a cell culture medium were further diluted in filtered distilled water (1:10) and agitated manually to maintain dispersion. Following this, particles were vacuum filtered onto a polycarbonate filter, which was then mounted on an aluminum stub and sputter-coated with gold−palladium. SEM images were taken on a Hitachi S4800 field emission scanning electron microscope (Hitachi, Tokyo, Japan) at magnifications of 15 000, 25 000, or 50 000×. For transmission electron microscopy (TEM), one drop of the diluted particle sample was placed on a Formvar-coated 200 mesh copper grid and evaporated overnight before imaging on a JEOL 1400 transmission electron microscope (JEOL, Tokyo, Japan).

Particle release of free iron in H_2O, the culture medium (BEGM), and the phagolysosome-like buffer was assessed using inductively coupled plasma-optical emission spectroscopy (ICP-OES) at CDC/NIOSH (Cincinnati, OH; calculated limit of quantification: 0.0566 μg/mL). Particles were serially diluted in 1 mL of water, BEGM, or phagolysosome-like buffer (prepared as previously described[49]) at the concentration of 20 μg/mL and then stored in a 37 °C incubator to replicate cell culture conditions. Particle-free vehicle controls were also prepared and stored. Then, 72 h later, particle suspensions were centrifuged (13 000 rpm for 10 min) and filtered (0.2 μm of PTFE, ThermoFisher), and the resulting supernatant was assessed for soluble iron content via ICP-OES. The percent of dissolved particle was calculated based on the beginning mass of particle and mass of detectable soluble iron.

Volume-weighted size distribution and effective density of particle suspensions in the medium (calculated as previously described[50]) were incorporated into a distorted grid (DG) fate and transport modeling algorithm in MatLab v.2006b developed at Harvard University[48,51,52] to assess cell deposited dose metrics as a function of exposure time.

Cell Culture and Exposure. Naïve Beas-2B cells (ATCC) were cultured in serum-free BEGM (basal medium with 1% penicillin/streptomycin, 0.4% bovine pituitary extract, 0.1% hydrocortisone, human epithelial growth factor, epinephrine, transferrin, insulin, retinoic acid, and triiodothyronine) from Lonza (Walkersville, MD) for a minimum of two passages before beginning exposures. Cells were passaged according to the ATCC guidelines. For acute exposures, Beas-2B were seeded at 10 000 cells per well in a 96-well plate (Corning). Then, 24 h postplating, the medium was aspirated out and replaced with specific particle treatments, or a particle-free vehicle control, which were prepared as described above, and serially diluted in BEGM to appropriate doses. Administered doses ranged from 0.2 μg/cm^2 (0.66 μg/mL) to 2.0 μg/cm^2 (6.6 μg/mL) for acute

DOI: 10.1021/acs.chemrestox.9b00118
Chem. Res. Toxicol. 2019, 32, 2382−2397

studies, and a subtoxic dose was selected for subchronic treatment based on these results and previous literature.[53]

For subchronic exposures, Beas-2B (passage 3) were seeded at 50 000 cells/well in 6-well plates (Corning), with four biological replicates per treatment group, from which at least three biological replicates were used for any subsequent assay. At 24 h postseeding, the medium was aspirated out and replaced with specific particle treatments, prepared as described above. All particle treatments were administered at 0.6 $\mu g/cm^2$ (2.88 $\mu g/mL$). Particle-free vehicle-exposed cells served as passage controls. The medium with particle treatments was replaced every 3 to 4 days. When cells were approximately 80−90% confluent (roughly once a week), cells were washed, trypsin/EDTA was released from the plate, and a random selection of cells was replated at a ψ seeding density of 50 000 cells/well in 75% of the total volume. Particle treatments were added directly to these wells approximately 3 h later in the remaining 25% volume. The remainder of cells from each passage/replating were used for cell transformation and ROS-related assays or frozen back for future studies.

Particle Uptake. Beas-2B (passage 3) were seeded at 50 000 cells/well in 6-well plates (Corning) and exposed to specific particle treatment 24 h later, as described above. The medium with particle treatment was replaced 3 days later. When cells were 80−90% confluent (1 week later), cells were washed, passaged, and prepared for transmission electron microscopy (TEM) as previously described.[54] Briefly, cells were suspended in Karnovsky's fixative and pelleted; then, the fixative was removed and replaced with 4% agarose. After congealment, excess agar was trimmed away, and fresh Karnovsky's fixative was added overnight. The pellet was rinsed (8% sucrose and 0.9% sodium chloride buffer), and then osmium teroxide was added. En bloc staining was done using 1% tannic acid and 0.5% uranyl acetate. The pellet was dehydrated using a graded series of ethanol, and then cells were embedded in epoxy resin and polymerized. Blocks were sectioned at 70 nm onto 200 mesh copper grids and stained (4% uranyl acetate and Reynold's Lead Citrate). Imaging was done at 1500−3000× or 10 000−50 000× magnification on a JEOL 1400 transmission electron microscope (JEOL, Tokyo, Japan).

Reactive Oxygen Species Production. For acute (18 and 24 h) and subchronic exposures (48, 62, 69, 76, 97, 104, 118, 125, 132, 145, and 195 days of continuous exposure), treated Beas-2B cells were seeded at 10 000 cells/well in a clear-bottom black 96-well plate (Corning), stained with 10 μM DCF-H and 1 μM Hoescht-33342 (Sigma-Aldrich, St. Louis, MO), and incubated at 37 °C for 30 min. Cells were washed once with BEGM, and imaged in warm PBS at 20× magnification, with 9 image sites per well. Imaging using DAPI and FITC filters were analyzed using high content screening on an ImageXpress Micro XLS apparatus with MetaXpress v5.3 software (Molecular Devices, San Jose, California). Using the MultiWavelength Application Module in MetaXpress, minimum/maximum cell diameters and minimum intensity thresholds were used to identify each nucleus (DAPI) and intracellular ROS (FITC). Masks were applied to identify cells for each imaged site positively. Only FITC masks containing a nucleus were included in the analysis. The integrated intensity of the fluorescent signal from each cell (evaluated using a cell mask) was calculated and averaged for quantification. Ten μM H_2O_2 treatment was used as a positive control for ROS detection, and particle-only controls were used to verify there was minimal particle interference (data not shown).

Cell Proliferation. Acute and subchronic exposures were done at previously indicated time points. Treated Beas-2B cells were plated at 10 000 cells/well in a 96-well plate with at least four technical replicates per biological replicate and treatment group. At appropriate time points, cells were incubated with WST-1 reagent (Sigma-Aldrich, St. Louis, MO) at a 1:10 dilution for 2 h; then, absorbance at 450 nm was measured using a spectrophotometer (SpectraMax, Molecular Devices, San Jose, California), according to manufacturer's instructions.

Attachment-Independent Colony Formation. A soft agar colony assay was conducted as previously described[34] at 55, 83, 111, 138, 174, and 202 days of continuous exposure. Briefly, the 0.5% w/v agar medium was prepared and plated in 6-well plates (1.25% Difco agar, 15% v/v fetal bovine serum, and growth supplements at concentrations consistent with the complete cell culture medium in 2× MEM). After the base layer was solidified, cells were suspended in 33% agar at 1×10^4 cells/well and slowly layered onto precast agar in triplicate 6-well plates. Plates were stored in a 37 °C incubator for 14 days, and colonies were digitally photographed under light microscopy (1.25×). Five representative pictures from each well were taken, totaling 15 pictures per biological replicate. Only colonies >50 μm in diameter were included in counts, which were done manually using ImageJ Grid and CellCounter plugins.

Intracellular Iron and Lysosome Counts. At select time points during subchronic exposure (91, 132, and 202 days), treated cells were seeded at 10 000 cells per well in a 96-well clear-bottom black plate (Corning). When cells were at least 70% confluent, Beas-2B were fluorescently stained with 1 μM PhenGreen SK, 1 μM Deep Red LysoTracker, and 1 μM Hoechst 33342. Plates were incubated at 37 °C for 30 min. Cells were washed once and imaged in warm Fluorobrite clear DMEM (ThermoFisher) at 20× magnification for intracellular iron and then 40× magnification for lysosome counts, with 9 imaging sites per well for each. Imaging (DAPI, FITC, and Cy5 filters) and analysis were done using the ImageXpress apparatus and MetaXpress software, as described above. Using this program, individual intracellular lysosomes were identified using minimum/maximum diameter masks, counted using the TransFlour HT module, and averaged per cell for each image site and treatment group. The integrated intensity of the PhenGreen fluorescent signal from each cell was calculated using a cell mask and averaged for the quantification of intracellular iron. The PhenGreen fluorescent signal from acute intracellular iron studies was measured using the Varioskan Lux fluorescent plate reader (excitation, 492 nm; emission, 517 nm). The PhenGreen fluorescent signal is quenched upon binding to free iron ions. Therefore, the inverse of the integrated intensity of the fluorescent signal was calculated using the nontreated control cell fluorescence as the threshold (F_0/F), as has been previously described.[55] Iron specificity of PhenGreen was assessed using $FeSO_4$ as a positive control and pyridoxal isonicotinoyl hydrazine (PIH, Sigma-Aldrich) as an intracellular iron chelation control).

γH2AX Assay for DNA Damage. Treated Beas-2B cells from subchronic exposure (91, 132, and 202 days) were seeded at 10 000 cells per well in a 96-well clear-bottom black plate (Corning). When cells were at least 70% confluent, the Beas-2B were fixed in 4% paraformaldehyde, permeabilized with 0.25% Triton-X, and then washed with PBS, all at ambient room temperature. Then, 48 h later, cells were incubated with 0.5% phosphorylated γH2AX primary antibody (1:250, Cell Signaling, Danvers, MA) for 1 h, washed in PBS, and fluorescently tagged using AlexaFlour-555 secondary antibody (1:500) and 1 μM Hoechst 33342. Imaging (at 20× magnification) and analysis were performed using the ImageXpress apparatus and MetaXpress software, as described above. Minimum/maximum cell diameters and minimum intensity thresholds were used to identify each nucleus (DAPI) as described above. The average nuclear intensity of the top 3% of nontreated cells was used as a threshold for positive or negative scoring of all cell treatments to determine the percentage of cells with positive γH2AX damage. H_2O_2 treatment (10 μM) was used as a positive control (data not shown).

Statistical Analyses. Data represent the mean ± SEM from three or more biological replicates and four or more technical replicates per biological replicate. Samples were normalized to the nontreated control for each biological replicate and then combined for all figures. Following normalization, samples were analyzed using a two-way ANOVA with Tukey's posthoc test for multiple comparisons to determine significance. Statistical significance is indicated in each figure as $*p < 0.05$, $**p < 0.01$, $***p < 0.001$, and $****p < 0.0001$. All statistical analyses were performed using GraphPad Prism Software (La Jolla, CA).

DOI: 10.1021/acs.chemrestox.9b00118
Chem. Res. Toxicol. 2019, 32, 2382−2397

Table 1. Colloidal/Physicochemical Characterization of Dispersed Nanoparticles after One Sonication[a]

ENM	d_{XRD} (nm)	SSA (m^2/g)	ζ (mV) [measured pH]	iron/iron oxide content (%)	d_H (Z avg, nm)	PDI	ρ_{ENM} (g/cm^3)	ρ_{EV} (g/cm^3)
nFe_2O_3	19.6	42	−8.63 [7.55]	100	2570	0.43	5.242	1.534
SiO_2-nFe_2O_3	21.3	49	−13 [7.54]	66	1895	0.28	5.242	1.273
SiO_2	19	147	−15.63 [7.58]	0	1774	0.16	2.648	1.08
gas metal arc mild steel welding fumes	15−45	nd	−10.49 [7.53]	80	1114	0.28	5.7	2.362
TiO_2	23	nd	−8.56 [7.59]	0	2085	0.17	4.26	1.391

[a]Primary particle size as determined by X-ray diffraction (d_{XRD}), surface area (SSA), hydrodynamic diameter (d_H), ζ potentials, iron/iron oxide content, polydispersity index (PDI), raw material density (ρ_{ENM}), and agglomerate effective density (ρ_{EV}) of all particle treatments in complete cell culture media (BEGM). nd: no data.

RESULTS

Particle Characterization. First, particles were evaluated for the agglomerate hydrodynamic diameter and ζ potential following preparation and sonication in sterilized water and then serial dilution in complete cell culture media (BEGM), using DLS (Table 1). All test particles had roughly similar primary particle diameters (d_{XRD} ranging from 15 to 45 nm) and ζ potentials (ranging from −15.63 to −8.84 mV) in BEGM, but with diverse agglomerate hydrodynamic diameters, ranging from 1114 nm (GMA-MS) to 2570 nm (nFe_2O_3).

Dispersed particle agglomerates were visualized using TEM (Figure 1A) and SEM (Figure 1B). SEM-EDX (Figure 1C) indicated an amorphous silica coating on SiO_2-nFe_2O_3 and also showed that GMA-MS particulates were primarily composed of insoluble iron and small amounts of other metals.

Acute Cytotoxicity Assessment. Next, the acute bioeffect of particle treatments (nFe_2O_3, SiO_2-nFe_2O_3, GMA-MS, SiO_2, and TiO_2) was evaluated. Reactive oxygen species (ROS) production and proliferative capacity were used as basic indicators of particle-induced changes in cell activity (Figure 2). Beas-2B cells were exposed to a range of administered doses (0.2−2.0 $\mu g/cm^2$) of particle treatments for up to 24 h, and ROS production and cell proliferation were assessed. For ROS production, treated Beas-2Bs showed a dose response for all particle treatments, with the greatest ROS response overall at 18 h postexposure (Figure 2A). The 2.0 $\mu g/cm^2$ administered dose of nFe_2O_3, GMA-MS, and TiO_2 all induced significantly elevated ROS production compared to nontreated controls at 18 h postexposure, with GMA-MS- and TiO_2-exposed cells retaining this elevated ROS at 24 h. There was no significant cell death induced by any particle treatments, and higher doses of SiO_2 and the lowest dose of TiO_2 induced significantly elevated proliferation at 24 h postexposure (Figure 2D). Intracellular iron was evaluated using the fluorophore, PhenGreen SK, and iron chelator, PIH. In Beas2B cells, the majority of iron is sequestered and not catalytically active. PIH, as a chelator, and PhenGreen, as a fluorescent marker, actively target chelatable iron within the cell's catalytically active labile iron pool,[56] as is indicated with $FeSO_4$ treatment, which was used as a control. There were no significant changes in intracellular iron across particle treatments at 18 or 24 h postexposure (Figure 3). Cells exposed to higher doses of GMA-MS (0.6 or 2.0 $\mu g/cm^2$ administered dose) showed a trend of elevated intracellular iron at 24 h postexposure. Overall, the acute treatment data supported 0.6 $\mu g/cm^2$ as a subtoxic dose for subchronic treatment.

Sub Chronic Cell Transformation. Based on previous *in vitro* and *in vivo* research, and results from the above acute experiments, an administered dose of 0.6 $\mu g/cm^2$ (2.88 μg/mL) was selected for the subchronic exposure. A recent study by Teeguarden et al.[53] exposed Balb/c mice to a similarly sized iron oxide (Fe_3O_4) particle via inhalation at 19.9 mg/m^3 over 4 h (80 mg h/m^3), which is slightly lower than the OSHA permissible exposure limit (PEL) for fine-sized Fe_2O_3 particles (14 mg/m^3 over 8 h or 112 mg h/m^3). Following the exposure, the target tissue dose in the bronchial region was calculated to be about 1 $\mu g/cm^2$. Previous research by our group[34] also indicated that, at a 0.6 $\mu g/cm^2$ administered dose, nFe_2O_3 induced a neoplastic-like cell transformation in primary human small airway epithelial cells. Therefore, in the present study, Beas-2B cells were exposed to this low dose (0.6 $\mu g/cm^2$) of nFe_2O_3, SiO_2-nFe_2O_3, GMA-MS, or particle controls (TiO_2, SiO_2) continuously for 6.5 months and assessed throughout for indications of neoplastic-like cell transformation, particularly at time points surrounding two, four, and six months.

Uncontrolled or dysregulated cell proliferation is a classic hallmark of cancer.[57] Therefore, this was used as an initial indicator of potential cell transformation throughout the exposure period (Figure 4). Beginning at 97 days (~3.25 months) of continuous exposure, nFe_2O_3-exposed cells had a trend of decreased proliferation, which began to increase at 118 days, as compared to nontreated controls. By 125 days (~4.5 months), the nFe_2O_3-exposed cells had almost a 2-fold significant increase in proliferation as compared to nontreated control cells. Elevated proliferation was maintained through the rest of the exposure period (6.5 months). GMA-MS-exposed cells followed a similar trend for this parameter, with significantly elevated proliferation (~1.25-fold) by 145 days (~5 months) of exposure, which was maintained through the rest of the exposure period, as compared to nontreated controls. However, SiO_2-nFe_2O_3-exposed cells had no significant changes in cell proliferation throughout the entire exposure period. TiO_2-exposed cells began to exhibit significantly decreased proliferation at 97 days of continuous exposure, which gradually increased until it became significantly elevated at 145 days. This elevation was maintained through the rest of the exposure period. SiO_2-exposed cells had significantly elevated cell proliferation at 125 days of continuous exposure, which then returned to be roughly similar to that of nontreated control cells by the end of the exposure period.

Attachment-independent colony formation is an indicator of neoplastic-like cell transformation because abnormal or neoplastic cells can continue to proliferate without attachment to a solid surface.[58] This was assessed using soft agar colony formation assay throughout the subchronic exposure period (Figure 5). At 55 days (~2 months) of continuous exposure, there were no significant changes in colony formation across treatment groups. nFe_2O_3- and GMA-MS-exposed cells had a

DOI: 10.1021/acs.chemrestox.9b00118
Chem. Res. Toxicol. 2019, 32, 2382−2397

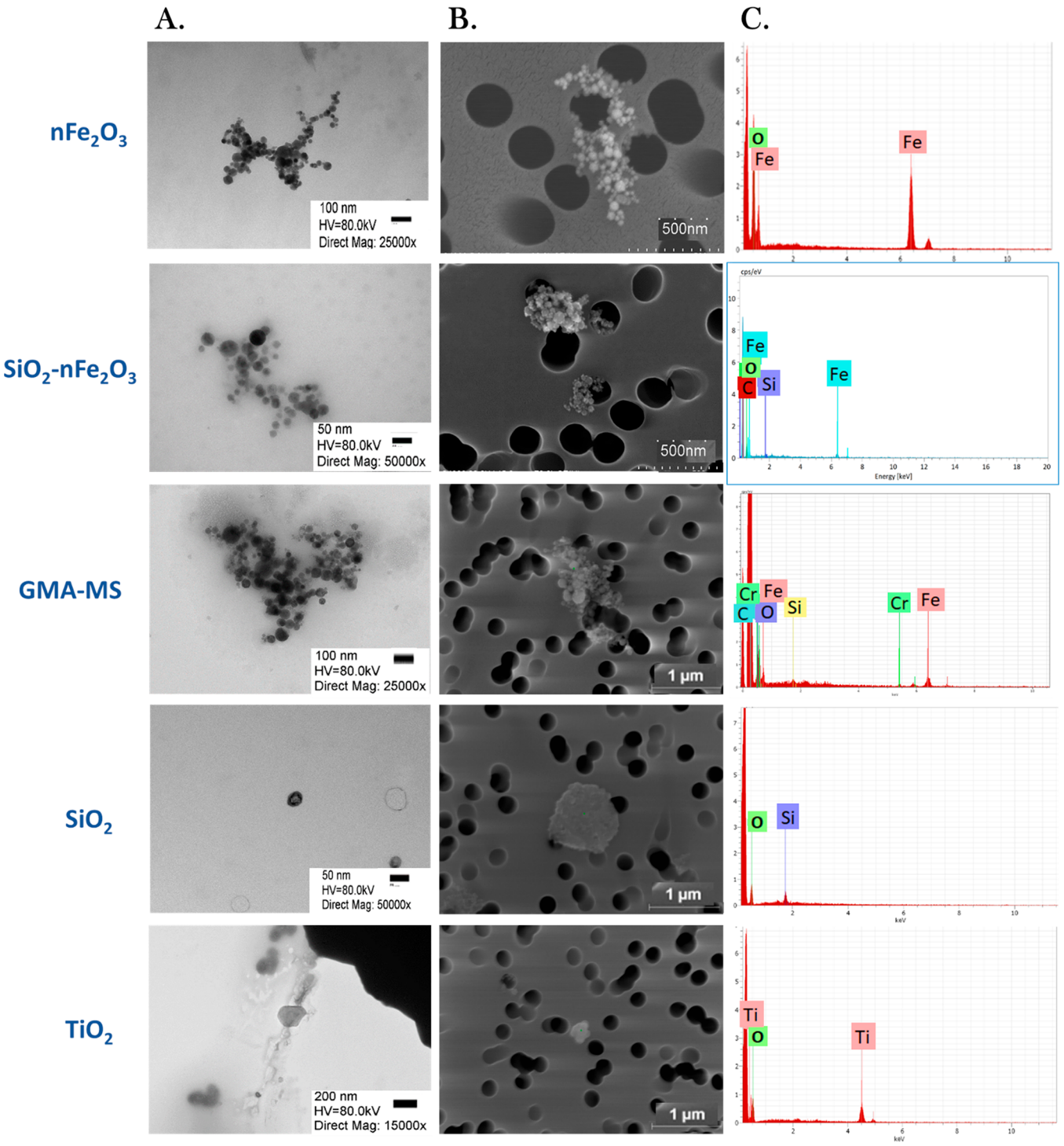

Figure 1. Representative SEM and TEM images of particle treatments. Particle agglomeration in a complete cell culture medium was visualized using (A) transmission electron microscopy (TEM), (B) scanning electron microscopy (SEM), and (C) SEM−energy-dispersive X-ray spectroscopy (SEM-EDX). For TEM, magnification ranged from 15 000 to 50 000×.

significant increase (1.2- and 1.4-fold) in colony number at 83 days (~2.75 months) postexposure, which was ablated by 111 days (~3.7 months). Colony number then became significantly elevated again (1.6-fold) at 138 days (~4.5 months) as compared to nontreated control cells, which was maintained through the remainder of the exposure period (202 days, ~6.5 months). TiO_2-exposed cells had a significant 1.3-fold increase in colony formation at 111 and 138 days, which then returned to be roughly similar to that of nontreated control cells by 174 days exposure and remained at baseline levels through the end of the exposure period. SiO_2-nFe_2O_3- and SiO_2-exposed cells had no significant changes in attachment-independent colony formation throughout the exposure period.

Subchronic Exposure-Induced Changes in Cell Response. Subchronically exposed cells were assessed for changes in intracellular iron, lysosome counts, ROS production, and DNA damage at key points during the subchronic exposure period. Intracellular iron and lysosome

DOI: 10.1021/acs.chemrestox.9b00118
Chem. Res. Toxicol. 2019, 32, 2382−2397

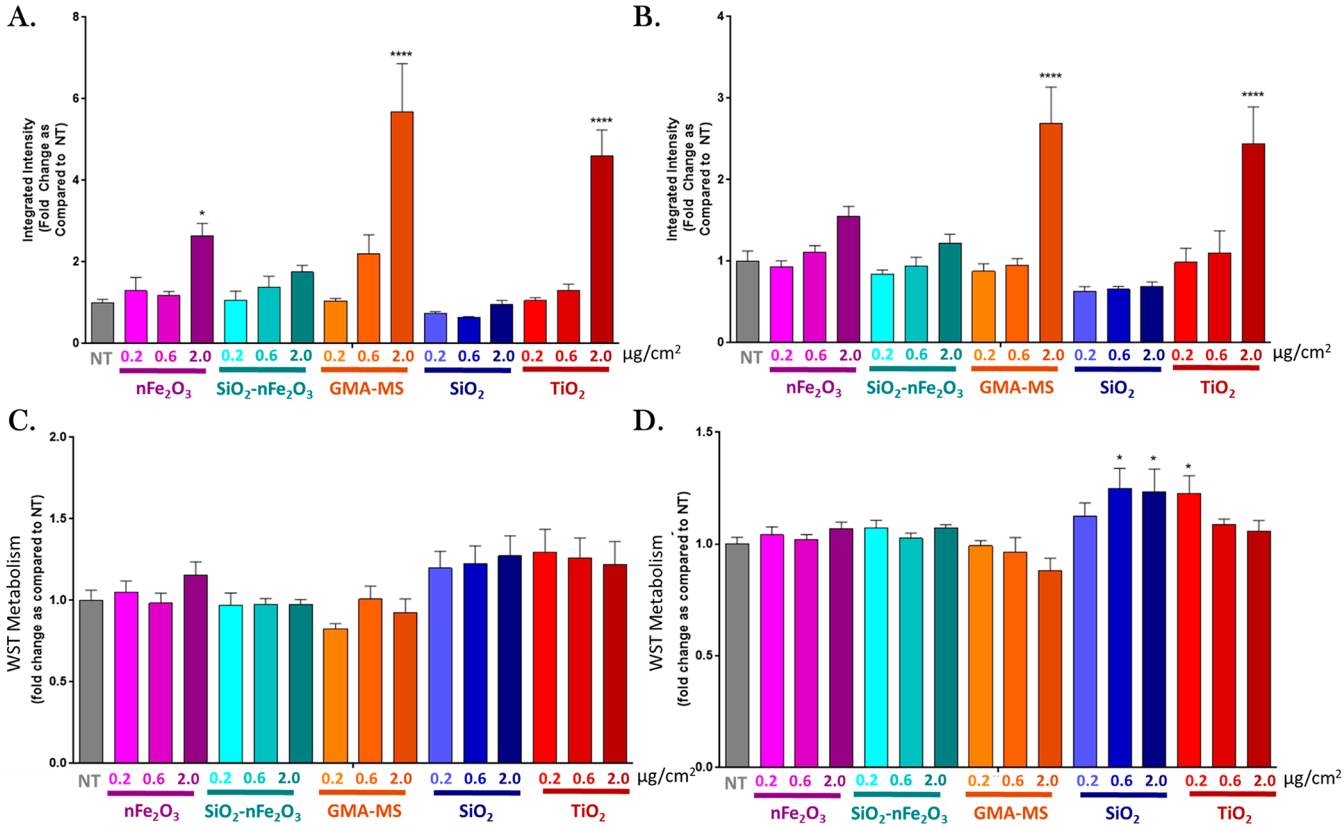

Figure 2. Acute particle-induced changes in ROS production (DCF assay) at (A) 18 and (B) 24 h and WST metabolism at (C) 18 and (D) 24 h postexposure. Doses refer to the administered dose. Error bars indicate the mean ± SEM (n = 3). *p < 0.05, ****p < 0.0001 from the nontreated control (NT).

counts were evaluated using PhenGreen SK and LysoTracker fluorescent staining and high content image analysis (Figure 6). At all three measured time points (91, 132, and 202 days of continuous exposure), nFe_2O_3-exposed cells had significantly decreased intracellular iron as compared to nontreated control cells (~70%, 55%, and 90% of nontreated control cells at 91, 132, and 202 days of continuous exposure, respectively). GMA-MS-exposed cells had significantly decreased intracellular iron at 91 days of continuous exposure only (~70% that of nontreated control cells) and then returned to be similar to nontreated control cells at 132 days, which was maintained through the end of the exposure period. GMA-MS-exposed cells also had significantly fewer average lysosomes per cell than nontreated controls at 202 days of continuous exposure, but all other treatment groups showed no significant changes in this parameter at this or any other time points measured.

ROS production was also assessed throughout the subchronic exposure period (Figure 7). At the first measured time point for this parameter (48 days/1.5 months continuous exposure), all treatment groups had significantly decreased ROS as compared to nontreated controls. nFe_2O_3-exposed cells showed a trend of increased ROS production at 104, 125, and 145 days, which then decreased to become less than that of production by nontreated control cells by the end of the exposure period. Both GMA-MS- and SiO_2-nFe_2O_3-exposed cells had slight and sometimes significantly decreased ROS production throughout the entire subchronic exposure period compared to nontreated controls. SiO_2- and TiO_2-exposed cells had no significant changes in ROS production throughout the exposure period, with the exception of the first time point measured (48 days).

Particle Dosimetry. A critical issue with *in vitro* nanoparticle exposures is the difficulty in ascertaining accurate dosimetry. Particle agglomeration and the settling rate will impact how the known administered dose may compare to actual delivered dose, while particle uptake may play a key role in the induction of adverse outcomes. First, previously calculated particle agglomeration (Table 1) and measured particle density were used to calculate the particle settling rate. Raw particle density is known to relate to effective density in a cell culture medium, and effective density is a key factor in the calculation of the *in vitro* particle deposition rate.[50]

These values, along with the hydrodynamic diameter, were used to model particle deposition (Table S1). All particles except for SiO_2 had greater than 90% particle deposition (average fraction deposited) within the first 24 h following treatment, whereas SiO_2 had roughly 70% deposition (average fraction deposited) by 24 h following exposure (0.6 $\mu g/cm^2$ administered dose or ~0.42 $\mu g/cm^2$ delivered dose). During the subchronic exposure period (6.5 months), particle suspensions in water were freshly prepared every 4 weeks and were sonicated before each exposure (every 3−4 days), followed by dilution in BEGM to 0.6 $\mu g/cm^2$ administrated dose (Figure 8). With repeated sonications (≤8 times), all particles decreased in the average agglomerate hydrodynamic diameter, but deposition remained >86% (>0.52 $\mu g/cm^2$ delivered dose for subchronic exposures), with the exception of SiO_2. For SiO_2, agglomerate size and deposition decreased roughly 7-fold over the course of eight repeated sonications.

DOI: 10.1021/acs.chemrestox.9b00118
Chem. Res. Toxicol. 2019, 32, 2382−2397

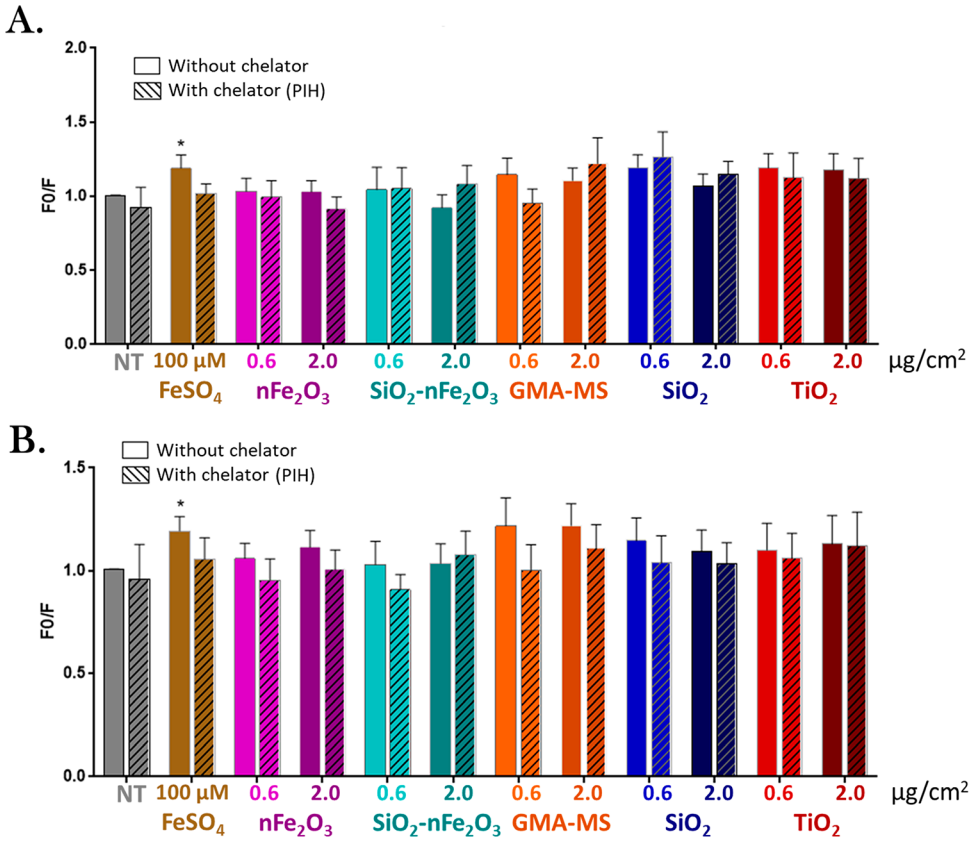

Figure 3. Acute particle-induced changes in intracellular iron (PhenGreen fluorescence) at (A) 18 and (B) 24 h. Doses refer to the administered dose. Error bars indicate the mean ± SEM (n = 4). Cross hatches indicate the addition of 100 μM pyridoxal isonicotinoyl hydrazine (PIH, iron chelator). In Beas2B cells, the majority of iron is sequestered and not catalytically active. PIH, as a chelator, and PhenGreen, as a fluorescent marker, actively target chelatable iron within the cell's catalytically active labile iron pool,[56] which is why it had minimal effect on acutely treated Beas2B, with the exception of FeSO4 treatment. F_0/F: the inverse integrated intensity of the fluorescent signal. *p < 0.05 from the same particle treatment without PIH chelation.

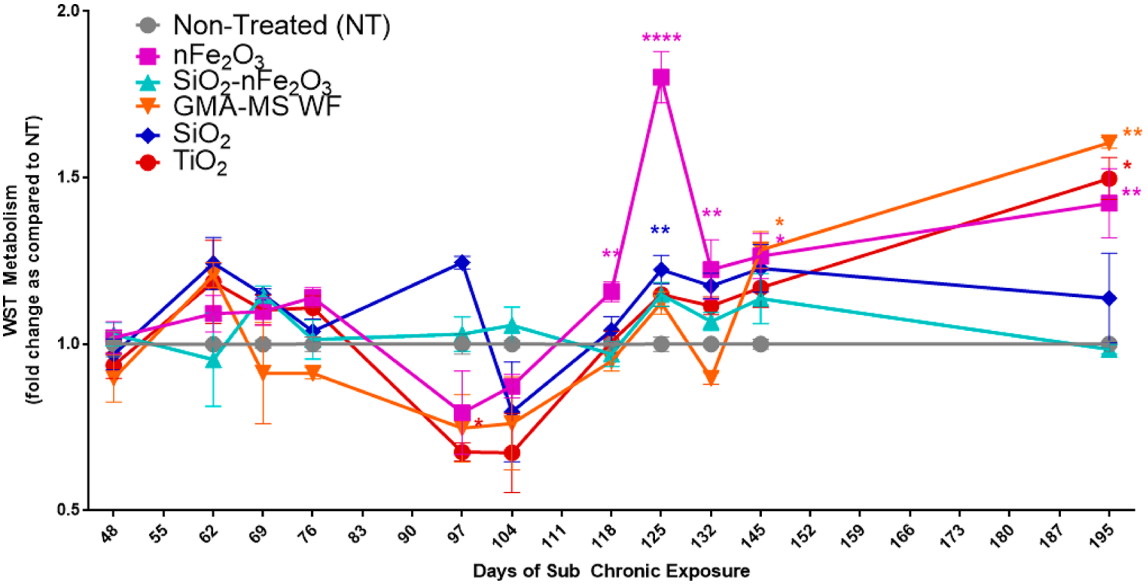

Figure 4. Cell proliferation throughout subchronic exposure to the 0.6 μg/cm^2 administered dose of specific particle treatment (~0.58 μg/cm^2 nFe_2O_3, ~0.54 μg/cm^2 SiO_2-nFe_2O_3, ~0.57 μg/cm^2 GMA-MS, ~0.24 μg/cm^2 SiO_2, or ~0.57 μg/cm^2 TiO_2 delivered dose). There were no significant changes in activity of nontreated control cells (Figure S1), so the fold change as compared to nontreated cells was calculated for each time point separately. *p < 0.05, **p < 0.01, ***p < 0.001, ****p < 0.0001 as compared to nontreated control cells at the same time point. Error bars indicate the mean ± SEM (n = 4).

DOI: 10.1021/acs.chemrestox.9b00118
Chem. Res. Toxicol. 2019, 32, 2382−2397

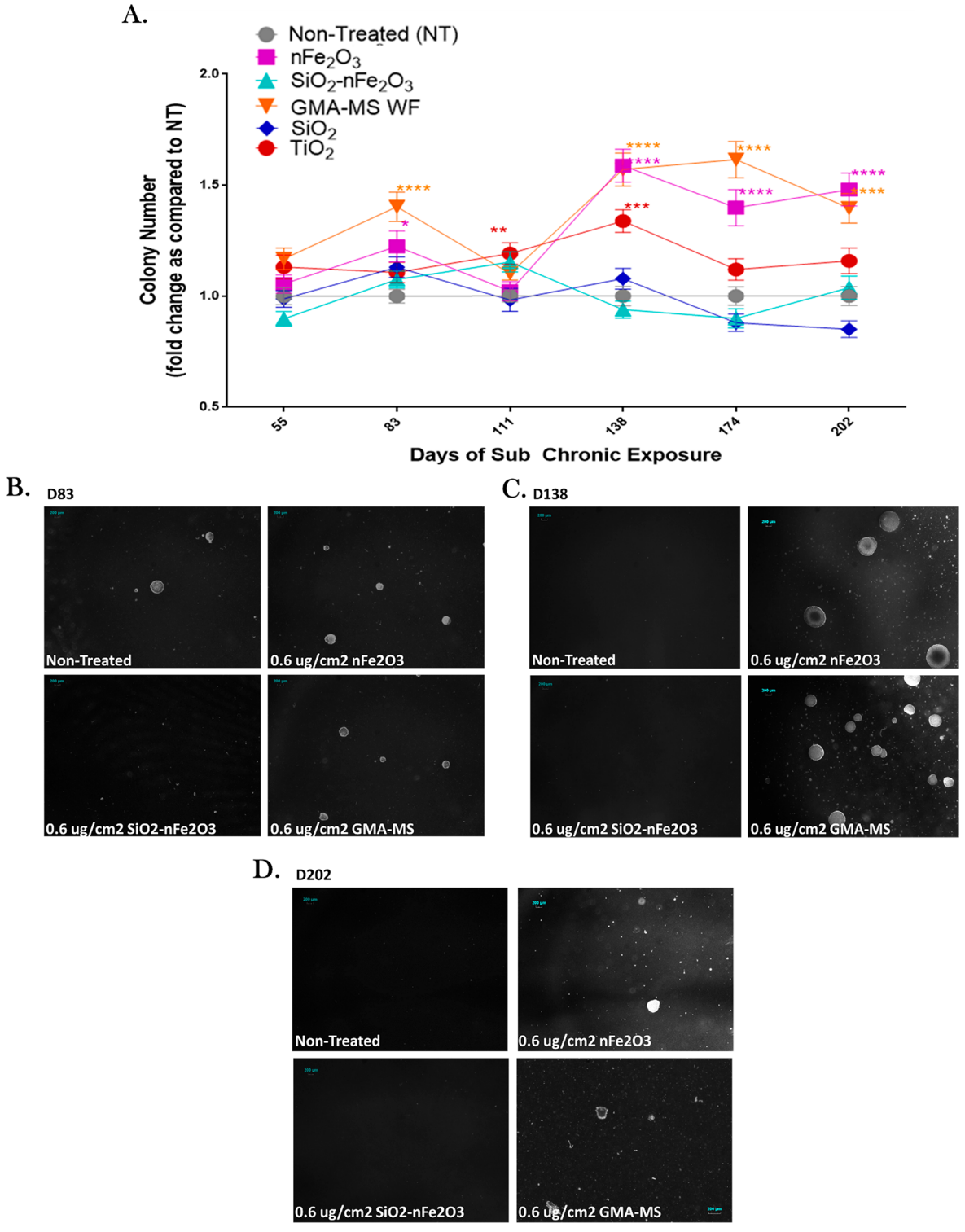

Figure 5. Attachment-independent colony formation throughout subchronic exposure to the 0.6 $\mu g/cm^2$ administered dose of specific particle treatment (~0.58 $\mu g/cm^2$ nFe_2O_3, ~0.54 $\mu g/cm^2$ SiO_2-nFe_2O_3, ~0.57 $\mu g/cm^2$ GMA-MS, ~0.24 $\mu g/cm^2$ SiO_2, or ~0.57 $\mu g/cm^2$ TiO_2 delivered dose). (A) Quantification of attachment-independent colonies followed by representative images of colonies from (B) 83 days, (C) 138 days, and (D) 202 days of continuous exposure. There were no significant changes in the activity of nontreated control cells (Figure S2), so the fold change as compared to nontreated cells was calculated for each time point separately. *$p < 0.05$, **$p < 0.01$, ***$p < 0.001$, ****$p < 0.0001$ as compared to nontreated control cells at the same time point. Error bars indicate the mean ± SEM ($n = 4$).

Qualitative particle uptake by Beas-2B cells was evaluated using TEM (Figure 9) following 1 week of continuous exposure, with two consecutive particle treatments. All particle treatments except SiO_2 were clearly shown to be taken up by cells and were shown encased in membrane-bound organelles, which were likely endosomes or phagolysosomes.

Particle dissolution of nFe_2O_3, GMA-MS, and SiO_2-nFe_2O_3 was assessed in sterilized Milli-Q water (pH 6.40), BEGM (pH

DOI: 10.1021/acs.chemrestox.9b00118
Chem. Res. Toxicol. 2019, 32, 2382−2397

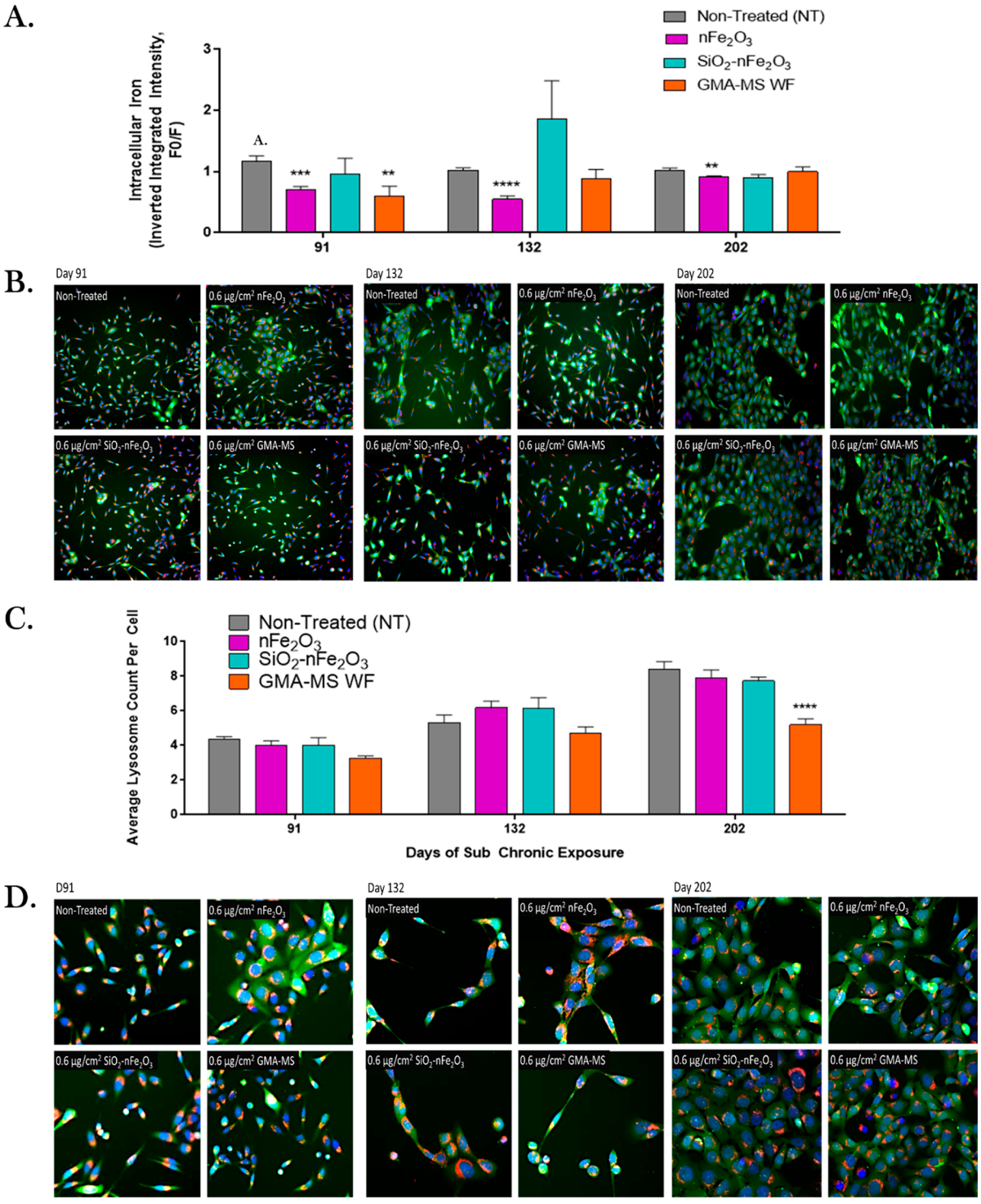

Figure 6. Intracellular iron and lysosome response during the subchronic exposure. (A) Quantification of intracellular iron fluorescent signal, (B) representative images of 20× fluorescent staining, (C) average lysosome count per cell, and (D) representative images of 40× fluorescent staining. Images were taken at key time points during subchronic exposure to the 0.6 $\mu g/cm^2$ administered dose of specific particle treatments (~0.58 $\mu g/cm^2$ nFe_2O_3, ~0.54 $\mu g/cm^2$ SiO_2-nFe_2O_3, ~0.57 $\mu g/cm^2$ GMA-MS, ~0.24 $\mu g/cm^2$ SiO_2, or ~0.57 $\mu g/cm^2$ TiO_2 delivered dose). For images, blue represents nuclear staining, green represents intracellular iron staining, and red represents lysosome staining. $^{**}p < 0.01$, $^{***}p < 0.001$, $^{****}p < 0.0001$ as compared to nontreated control cells. Error bars: mean ± SEM ($n = 3$). F_0/F: the inverse integrated intensity of the fluorescent signal.

7.46), or a phagolysosome-like buffer (pH 4.55) over 72 h by ICP-OES (Figure 10). In both water and BEGM, SiO_2-nFe_2O_3 had the greatest iron release as compared to other particle treatments. In phagolysosome-like buffer, GMA-MS had the greatest iron release, while nFe_2O_3 had the least. However, overall particle dissolution was relatively minimal, with the maximum dissolution at only 1.2% over 72 h.

DISCUSSION

Within the context of a subchronic *in vitro* exposure model, the present study showed a particle type and time-dependent

DOI: 10.1021/acs.chemrestox.9b00118
Chem. Res. Toxicol. 2019, 32, 2382−2397

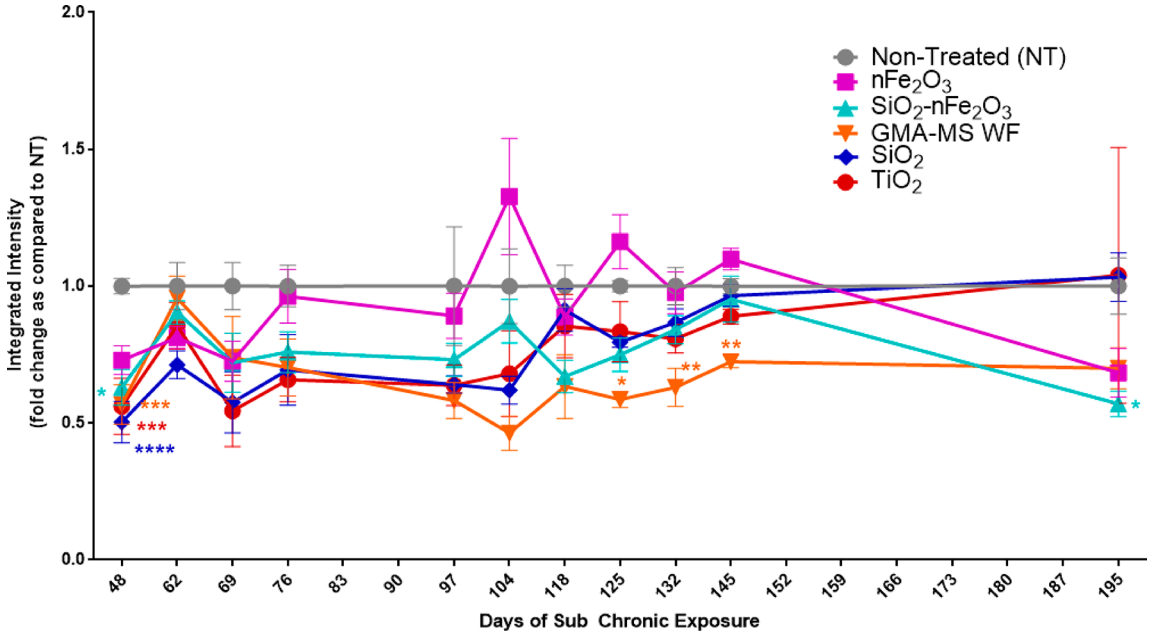

Figure 7. ROS production throughout subchronic exposure to the 0.6 $\mu g/cm^2$ administered dose of specific particle treatments (~0.58 $\mu g/cm^2$ nFe_2O_3, ~0.54 $\mu g/cm^2$ SiO_2-nFe_2O_3, ~0.57 $\mu g/cm^2$ GMA-MS, ~0.24 $\mu g/cm^2$ SiO_2, or ~0.57 $\mu g/cm^2$ TiO_2 delivered dose). There were no significant changes in ROS production of nontreated control cells (Figure S3), so the fold change as compared to nontreated cells was calculated for each time point separately. *$p < 0.05$, **$p < 0.01$, ***$p < 0.001$, ****$p < 0.0001$ as compared to nontreated control cells at the same time point. Error bars indicate the mean ± SEM ($n = 4$). Genomic instability and DNA damage are known to be key events associated with carcinogenesis.[59] There are several types of DNA damage that have been implicated in carcinogenesis adverse outcome pathways, such as double-stranded DNA damage, which is known to have a critical impact on cell phenotype.[60,61] To assess double-stranded DNA damage of the transformed cells, γH2AX fluorescence was evaluated at key time points during the subchronic exposure period (Figure 8) as an indicator of double-stranded DNA breaks.[62] At 132 days (~4.5 months) of continuous exposure, there were significantly more nFe_2O_3-exposed cells that were γH2AX positive as compared to SiO_2-nFe_2O_3-treated cells. By 202 days of continuous exposure, nFe_2O_3-exposed cells had significantly elevated γH2AX as compared to both nontreated and SiO_2-nFe_2O_3-treated cells. GMA-MS cells also showed significant DNA damage at 202 days of continuous exposure as compared to nontreated control cells.

neoplastic-like cell transformation. Long-term exposure to a 0.6 $\mu g/cm^2$ administered dose (~0.58 $\mu g/cm^2$ delivered dose) of nFe_2O_3 induced neoplastic-like transformation in Beas-2B cells beginning at 4−4.5 months, which was associated with decreases in intracellular iron, minimal changes in ROS production, and significantly elevated cell proliferation, colony formation, and double-stranded DNA damage. The observed response was similar to that of GMA-MS-exposed cells (0.6 $\mu g/cm^2$ administered dose, ~0.57 $\mu g/cm^2$ delivered dose). Conversely, Beas-2B cells exposed to amorphous silica-coated nFe_2O_3 particles (SiO_2-nFe_2O_3, 0.6 $\mu g/cm^2$ administered dose, ~0.54 $\mu g/cm^2$ delivered dose) did not undergo a neoplastic-like transformation, nor exhibit significant changes in any of the above-measured parameters.

Acute assessment of cytotoxicity and ROS production (Figure 2) showed that nFe_2O_3, GMA-MS, and TiO_2 exposure induced significantly elevated ROS production at 18 h, which was maintained through 24 h for GMA-MS and TiO_2 treatments, at the highest dose used (2.0 $\mu g/cm^2$). However, this influx did not have a significant impact on acute cytotoxicity or cell proliferation for nFe_2O_3 or GMA-MS. There were also no significant changes in intracellular iron (Figure 2) across particle treatment groups, although GMA-MS induced a trend of increased intracellular iron at 24 h postexposure at both the 0.6 and 2.0 $\mu g/cm^2$ administered dose.

Based on the presented acute response, target lung tissue dose determined from *in vivo* results,[53] and previous cell transformation data,[63] a subtoxic administered dose (0.6 $\mu g/cm^2$) was selected for subchronic exposure. Such low-dose/long-term exposure is more physiologically representative of occupational and environmental exposure conditions than a high-dose/acute exposure scenario and may be more likely to contribute to the human development of chronic conditions.[64] Throughout the subchronic exposure period, cells were assessed for neoplastic-like transformation, using cell proliferation (Figure 4) and attachment-independent colony formation (Figure 5) as primary indications. Uncontrolled or dysregulated cell proliferation can indicate some type of abnormal cell phenotype,[65] while a soft agar colony formation assay is the recommended technique by OECD to assess continued proliferation when cells are plated in nonadherent conditions,[58] which is a hallmark of abnormal or cancer-like phenotype in cells.[65] Both nFe_2O_3 and GMA-MS-exposed-cells followed a similar trend of decreased proliferation at roughly 3−3.5 months, which became significantly elevated by 4.5−5 months, and was maintained through the rest of the 6.5-month exposure period. The initial lower proliferation observed in the first few months of exposure may have indicated some type of chronic cell injury or stress, leading to cell adaptation, and ultimately resulting in significantly elevated proliferation and overall cell transformation by the end of the exposure period. The 4.5−5-month time point, when elevated cell proliferation was first observed, coincided with significant elevation of attachment-independent colony formation, again indicating particle-induced cell transformation by nFe_2O_3 and GMA-MS. For nFe_2O_3 exposure, this trend has been previously reported[34] and, at the time, was suggested to be attributable to chronic

DOI: 10.1021/acs.chemrestox.9b00118
Chem. Res. Toxicol. 2019, 32, 2382−2397

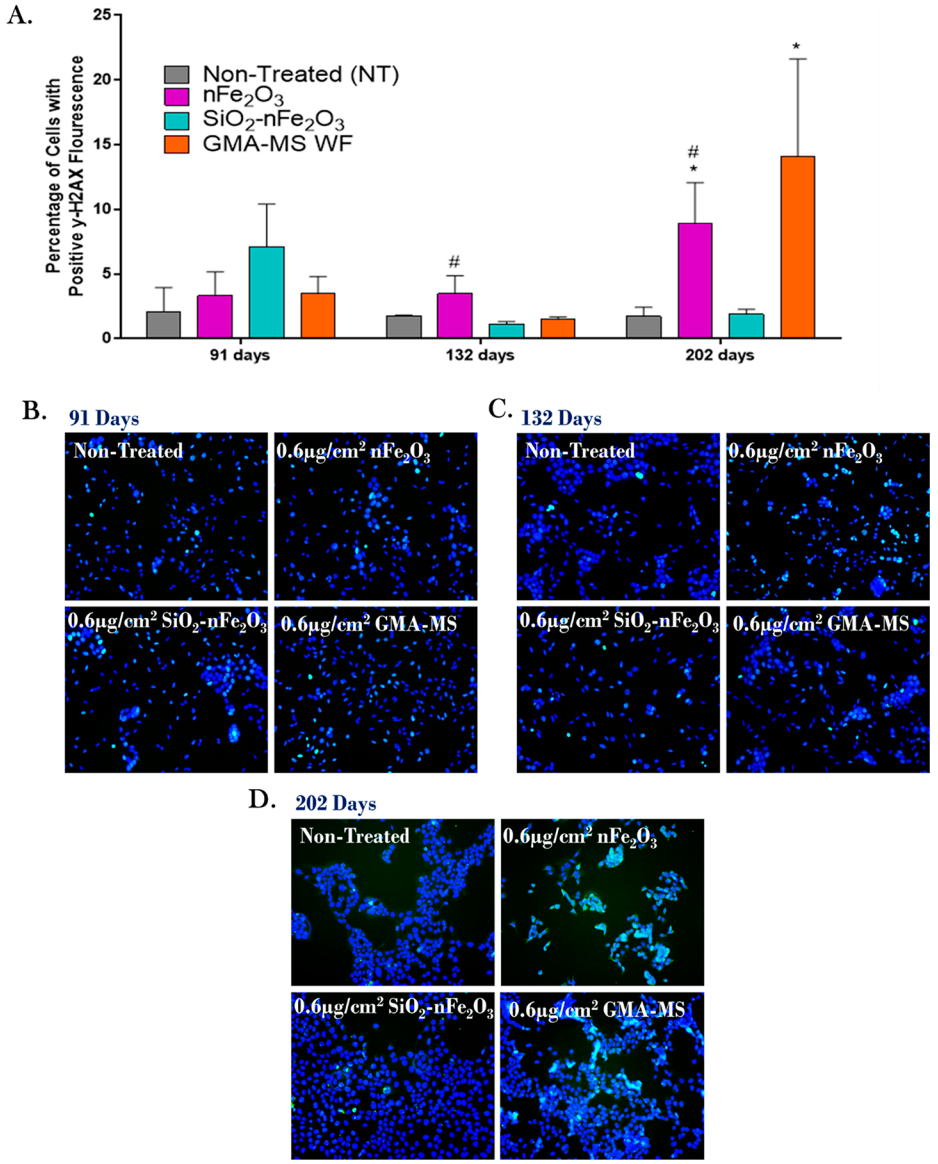

Figure 8. Double-stranded DNA damage (p-γH2AX) at key points during subchronic exposure to 0.6 μg/cm^2 of selected particle treatments (~0.58 μg/cm^2 nFe_2O_3, ~0.54 μg/cm^2 SiO_2-nFe_2O_3, ~0.57 μg/cm^2 GMA-MS, ~0.24 μg/cm^2 SiO_2, or ~0.57 μg/cm^2 TiO_2 delivered dose). (A) Quantification of the integrated intensity of fluorescent signals, representative images of fluorescent staining at (B) 91 days, (C) 132 days, and (D) 202 days of continuous exposure. *$p < 0.05$ as compared to nontreated control cells at the same time point. #$p < 0.05$ as compared to SiO_2-nFe_2O_3-exposed cells at the same time point. Error bars indicate the mean ± SEM ($n = 3$).

particle injury, which may have resulted in chronically stressed cells and resulting adaptations.

TiO_2 exposure induced a similar trend in cell proliferation as GMA-MS and nFe_2O_3, but without a sustained neoplastic-like transformation. TiO_2-exposed cells also showed increased attachment-independent colony formation at 4.5−5 months, but this effect was gone by the end of the exposure period, even though cell proliferation remained elevated. This suggested that TiO_2 may have the potential to induce cell transformation, but a more transient kind. This is mirrored in the current literature, which has shown TiO_2 exposure to be associated with *in vitro* cytotoxicity[66,67] and *in vivo* tumorigenesis only at high doses.[68]

nFe_2O_3- and GMA-MS-induced cell transformation was hypothesized to be reliant on particle-induced changes in intracellular iron, ROS production, and double-stranded DNA damage. It is generally believed that if a particle is engulfed by the cell via phagocytosis or endocytosis, the resulting phagosome will fuse with a lysosome for degradation. Once in this acidic environment, iron-containing particles may dissolve and release free iron ions into the cell's labile iron pool. This increase in catalytically available iron can participate in the Fenton reaction and generate ROS,[69,70] which is known to induce DNA lesions,[71] and may ultimately result in the observed neoplastic-like phenotype predicted with subchronic nFe_2O_3 or GMA-MS exposure. Therefore, this proposed mechanism was evaluated using changes in intracellular iron, ROS production, and double-stranded DNA damage at key points during the subchronic exposure for nFe_2O_3-, SiO_2-nFe_2O_3-, or GMA-MS-exposed cells, which, to our knowledge, has not been previously reported for any of these particles. However, our data showed that nFe_2O_3 and GMA-MS induced decreased intracellular iron and minimal changes in ROS production, but still induced significant double-stranded DNA

DOI: 10.1021/acs.chemrestox.9b00118
Chem. Res. Toxicol. 2019, 32, 2382−2397

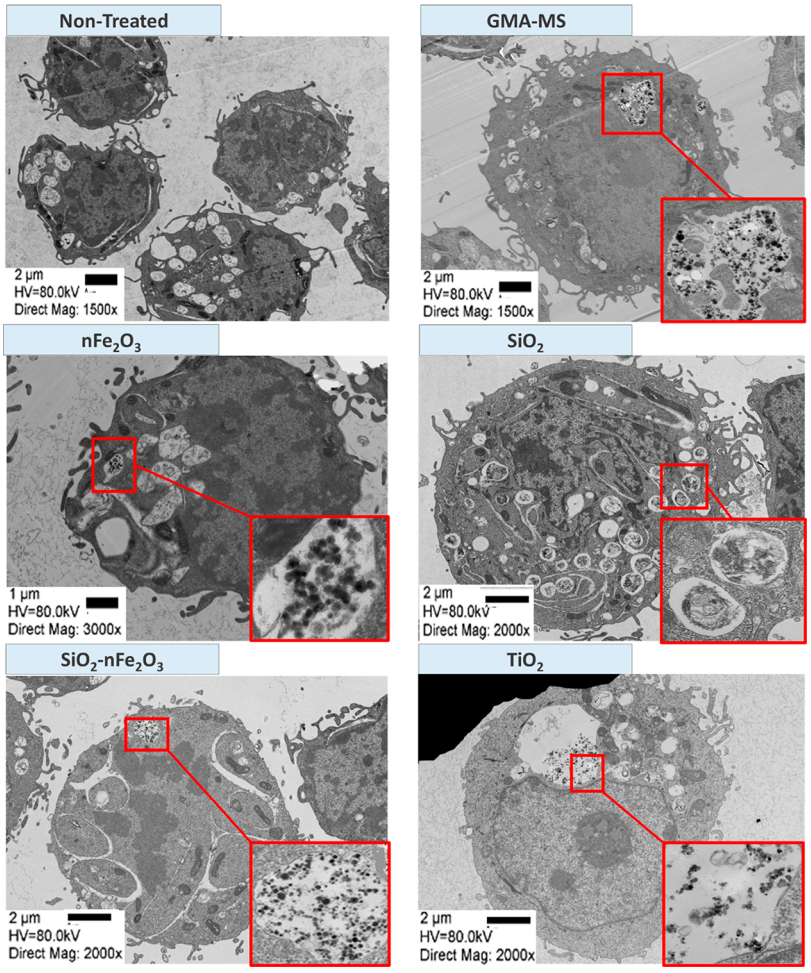

Figure 9. Representative transmission electron microscopy (TEM) images of Beas-2B uptake of particles following 1 week of continuous exposure (two consecutive particle treatments). Arrows refer to the location of higher magnification images.

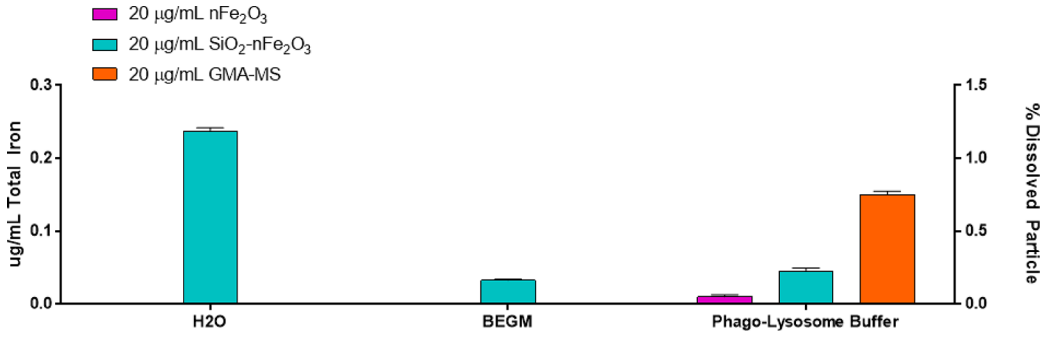

Figure 10. Particle dissolution following a 72 h suspension in sterilized water (pH 6.40), complete cell culture medium (BEGM, pH 7.46), or phagolysosome-like buffer (pH 4.55) by ICP-OES. Error bars indicate the mean ± SEM (n = 3). Limit of quantification: 0.0283 μg/mL. Limit of detection: 0.0089 μg/mL, with a maximum of 1.5% dissolved particle measured over 72 h.

damage. Therefore, the observed subchronic effects were likely not due to an influx of intracellular iron, but rather some kind of alternative mechanism. The minimal changes in ROS production observed by nFe_2O_3- and GMA-MS-exposed cells align with some previous literature, which has shown human lung adenocarcinoma cells to have minimal oxidative stress response with IONP exposure, even though the exposure still resulted in increased DNA damage.[72] Cadmium, a heavy metal which is a known carcinogen, induced decreased oxidative stress[73] and minimal changes in related gene expression[74] with low-dose/long-term exposure, as well. For cadmium, adaptation and tolerance to oxidative stress were believed to be critical mechanisms involved in its overall toxicity and carcinogenic capacity.[75] Arsenic, another heavy metal, was reported to have a similar effect. Arsenic-transformed Beas-2B cells exhibited a decrease in ROS generation, which was posited to be responsible for observed increases in cell growth and colony formation.[76]

However, the underlying mechanism of carcinogenic agent-induced cell transformation is not totally understood. The results presented here, as well as similarly conducted low-dose/long-term exposure studies, suggest other mechanisms

DOI: 10.1021/acs.chemrestox.9b00118
Chem. Res. Toxicol. 2019, 32, 2382−2397

involved in the nFe_2O_3 induced-cell transformation and DNA damage beyond the hypothesized intracellular iron-ROS-DNA damage pathway, such as a direct nanoparticle surface interaction with exposed cells, cellular uptake efficiency, and intracellular distribution of the engulfed particles, which we are currently investigating in our lab.

Subchronic GMA-MS exposure induced a similar response in cells compared to nFe_2O_3 treatment. Previous GMA-MS *in vivo* pulmonary exposure has shown minimal inflammatory or oxidative stress response, and no changes in iron homeostasis markers,[77] even though long-term exposure did induce genotoxicity[78] and tumor formation.[36] This aligns with the presented *in vitro* GMA-MS-induced cell transformation, which occurred without direct increases in intracellular iron or ROS production. GMA-MS-exposed cells also had a decreasing average number of lysosomes per cell over time (Figure 6C), suggesting cellular changes in autophagy, which have been previously shown to act as a protective mechanism in some types of particle-induced cell transformation.[79] Autophagy dysfunction as a potential underlying mechanism is also under further investigation in our lab.

As was hypothesized, compared to nFe_2O_3 treatment, SiO_2-nFe_2O_3-exposed cells did not show any significant changes in cell proliferation or attachment-independent colony formation throughout the subchronic exposure period and also did not exhibit any significant changes in intracellular iron, ROS production, or DNA damage. This suggested the protective capacity of the amorphous silica coating by reducing the overall cell interaction with nFe_2O_3. Many researchers have shown the utility of using a surface coating to alter particle function.[80−82] Previous studies have also shown the potential for an amorphous silica coating to reduce or postpone inflammatory outcomes *in vivo* with other types of nanometal oxides,[83] but this has not been previously shown for SiO_2-nFe_2O_3 within the context of a low-dose/long-term *in vitro* exposure model, as is presented here.

A complicating factor for *in vitro* nanotoxicology is the lack of information regarding dosimetry. In the present study, when able to do so, we evaluated how the known administered dose compared to the actual delivered dose of test particles. If the known administered dose and calculated delivered dose to the cells vary significantly, this may be able to account for unexpected observed cell response. Particle characterization was done in the present study via DLS (Table 1), SEM-EDX, and TEM (Figures 1 and 9) in conditions that replicated those of exposure. The delivered dose of each particle in a complete cell culture medium (BEGM) was calculated using the distorted grid (DG) dosimetry model. Due to the extended exposure period (6.5 months), particle suspensions in Milli-Q water were freshly prepared every 4 weeks, and sonicated before each particle treatment (every 3−4 days). This repeated sonication (≤8 times) affected the average agglomerate hydrodynamic diameter for particle treatments. However, regardless of hydrodynamic diameter, all test particles except amorphous SiO_2 had >86% deposition within the first 24 h after exposure (Table S1). Previous research has shown that particle settling rates are dependent on a complex interplay of each particle's effective density, protein corona formation, and medium composition and viscosity.[84] The cell culture medium used in this study (BEGM) was serum-free and had a low density/viscosity. This, combined with the relatively high effective density of the metal-oxide particles, resulted in rapid particle deposition regardless of agglomerate size or the number of sonications. Amorphous SiO_2, however, had a much lower effective density, as well as steadily decreasing agglomerate size with repeated sonications, which resulted in the observed low deposition (≤70% after 24 h). Cells treated with amorphous SiO_2 did not receive a similar deposited dose as compared to other particle treatments; therefore, no definitive conclusions about the potential toxicity of amorphous SiO_2 can be made compared to other treatments used in the present study. Information about amorphous SiO_2 toxicity can be inferred from previous research, which has shown the overall benign[85,86] or protective[83,85,87−89] qualities of amorphous SiO_2, especially when used as a coating for other types of metallic nanoparticles. Furthermore, in the present study, SiO_2-coated nFe_2O_3 had a similar deposition to its uncoated counterpart (nFe_2O_3), resulting in the direct contact of cells with amorphous SiO_2, but did not induce neoplastic-like cell transformation, which may further support the potentially protective/benign qualities of amorphous SiO_2. However, this example clearly emphasizes the importance of thorough particle characterization before exposure begins to ensure consistent dosing each time.

CONCLUSIONS

Subchronic *in vitro* exposure to nFe_2O_3 (~0.58 $\mu g/cm^2$ delivered the dose, for 6.5 months) induced a neoplastic-like cell transformation in human lung bronchial epithelial cells (Beas-2B), as characterized by elevated cell proliferation, increased attachment-independent colony formation, and induction of DNA damage. An amorphous silica-coated but otherwise identical nFe_2O_3 particle (SiO_2-nFe_2O_3, ~0.54 $\mu g/cm^2$ delivered dose) had markedly diminished neoplastic-like cell transformation, as indicated by no significant changes in any of the parameters described above.

GMA-MS subchronic exposure (~0.57 $\mu g/cm^2$ delivered dose) induced a neoplastic-like cell transformation in Beas-2B cells similar to that induced by nFe_2O_3 exposure, which was also associated with the induction of double-stranded DNA damage, but overall decreased ROS production and no significant changes in intracellular iron. Overall, this suggests that ROS may play a limited and not critical role in particle-induced neoplastic-like transformation *in vitro* or carcinogenesis *in vivo*.

This study provides support for physicochemical property-dependent modes of toxicity for nanometal oxide-induced carcinogenic potential and helps establish a "safe by design" hazard reduction strategy for emerging nanotechnology. Furthermore, this study gives evidence for the utility of a low-dose/long-term *in vitro* exposure model to assess the risk of cancer-related outcomes for occupationally relevant nanometal oxide exposures.

ASSOCIATED CONTENT

Supporting Information

The Supporting Information is available free of charge on the ACS Publications website at DOI: 10.1021/acs.chemrestox.9b00118.

Particle dosimetry with repeated sonications; nontreated cell proliferation throughout subchronic exposure, using raw absorbance of WST1 assay as a measurement; attachment-independent colony formation of nontreated control cells throughout subchronic exposure, shown in raw colony counts; ROS production of nontreated

DOI: 10.1021/acs.chemrestox.9b00118
Chem. Res. Toxicol. 2019, 32, 2382−2397

control cells throughout subchronic exposure, shown in raw fluorescent units (PDF)

AUTHOR INFORMATION

Corresponding Authors

*E-mail: tkornberg@cdc.gov.

*E-mail: lmw6@cdc.gov.

ORCID

Tiffany G. Kornberg: 0000-0002-6535-3128

Author Contributions

T.G.K. and L.R. were responsible for the overall study design. T.G.K. performed the majority of experiments, with contributions for subchronic experiments by L.R. and J.C. R.D. conducted dosimetric analysis. P.D. provided particles and dosimetry analysis methods. Y.R. participated in the study plan design and manuscript writing. T.A.S. participated in overall study design and manuscript writing. All authors have given approval to the final version of the manuscript.

Funding

This study was supported by NIOSH/NTRC funding.

Notes

The authors declare no competing financial interest.

ACKNOWLEDGMENTS

The authors would like to acknowledge Ronnee Andrews for all ICP-OES data. The authors would like to acknowledge Sherri Friend for all SEM and TEM images. The authors would like to acknowledge Sherry Xu for assistance with MatLab analysis.

ABBREVIATIONS

IONP, iron oxide nanoparticles; GMA-MS, gas metal arc mild steel welding fumes; ROS, reactive oxygen species; nd, no data

REFERENCES

(1) Starmans, L. W. E., Burdinski, D., Haex, N. P. M., Moonen, R. P. M., Strijkers, G. J., Nicolay, K., and Grüll, H. (2013) Iron Oxide Nanoparticle-Micelles (ION-Micelles) for Sensitive (Molecular) Magnetic Particle Imaging and Magnetic Resonance Imaging. *PLoS One 8* (2), No. e57335.

(2) Unterweger, H., Tietze, R., Janko, C., Zaloga, J., Lyer, S., Taccardi, N., Goudouri, M., Hoppe, A., Eberbeck, D., Schubert, D., et al. (2014) Development and Characterization of Magnetic Iron Oxide Nanoparticles with a Cisplatin-Bearing Polymer Coating for Targeted Drug Delivery. *Int. J. Nanomed. 9*, 3659.

(3) Gonçalves, M., Guerreiro, M. C., de Oliveira, L. C. A., and de Castro, C. S. (2013) A Friendly Environmental Material: Iron Oxide Dispersed over Activated Carbon from Coffee Husk for Organic Pollutants Removal. *J. Environ. Manage. 127*, 206−211.

(4) Sotiriou, G. A., Singh, D., Zhang, F., Chalbot, M.-C. G., Spielman-Sun, E., Hoering, L., Kavouras, I. G., Lowry, G. V., Wohlleben, W., and Demokritou, P. (2016) Thermal Decomposition of Nano-Enabled Thermoplastics: Possible Environmental Health and Safety Implications. *J. Hazard. Mater. 305*, 87−95.

(5) Singh, D., Schifman, L. A., Watson-Wright, C., Sotiriou, G. A., Oyanedel-Craver, V., Wohlleben, W., and Demokritou, P. (2017) Nanofiller Presence Enhances Polycyclic Aromatic Hydrocarbon (PAH) Profile on Nanoparticles Released during Thermal Decomposition of Nano-Enabled Thermoplastics: Potential Environmental Health Implications. *Environ. Sci. Technol. 51* (9), 5222−5232.

(6) DeLoid, G. M., Wang, Y., Kapronezai, K., Lorente, L. R., Zhang, R., Pyrgiotakis, G., Konduru, N. V., Ericsson, M., White, J. C., De La Torre-Roche, R., Xiao, H., McClements, D. J., and Demokritou, P. (2017) An Integrated Methodology for Assessing the Impact of Food Matrix and Gastrointestinal Effects on the Biokinetics and Cellular Toxicity of Ingested Engineered Nanomaterials. *Part. Fibre Toxicol. 14* (1), 1.

(7) Pirela, S. V., Sotiriou, G. A., Bello, D., Shafer, M., Bunker, K. L., Castranova, V., Thomas, T., and Demokritou, P. (2015) Consumer Exposures to Laser Printer-Emitted Engineered Nanoparticles: A Case Study of Life-Cycle Implications from Nano-Enabled Products. *Nanotoxicology 9* (6), 760−768.

(8) Servin, A. D., and White, J. C. (2016) Nanotechnology in Agriculture: Next Steps for Understanding Engineered Nanoparticle Exposure and Risk. *NanoImpact 1*, 9−12.

(9) De La Torre Roche, R., Pagano, L., Majumdar, S., Eitzer, B. D., Zuverza-Mena, N., Ma, C., Servin, A. D., Marmiroli, N., Dhankher, O. P., and White, J. C. (2018) Co-Exposure of Imidacloprid and Nanoparticle Ag or CeO2to Cucurbita Pepo (Zucchini): Contaminant Bioaccumulation and Translocation. *NanoImpact 11*, 136−145.

(10) Cai, F., Wu, X., Zhang, H., Shen, X., Zhang, M., Chen, W., Gao, Q., White, J. C., Tao, S., and Wang, X. (2017) Impact of TiO2nanoparticles on Lead Uptake and Bioaccumulation in Rice (Oryza Sativa L.). *NanoImpact 5*, 101−108.

(11) Wild, P., Bourgkard, E., and Paris, C. (2009) Lung Cancer and Exposure to Metals: The Epidemiological Evidence. *Methods Mol. Biol. 472*, 139−167.

(12) Baldauf, R. W., Devlin, R. B., Gehr, P., Giannelli, R., Hassett-Sipple, B., Jung, H., Martini, G., McDonald, J., Sacks, J. D., and Walker, K. (2016) Ultrafine Particle Metrics and Research Considerations: Review of the 2015 UFP Workshop. *Int. J. Environ. Res. Public Health 13* (11), 1054.

(13) Kobayashi, N., Naya, M., Endoh, S., Maru, J., Yamamoto, K., and Nakanishi, J. (2009) Comparative Pulmonary Toxicity Study of Nano-TiO(2) Particles of Different Sizes and Agglomerations in Rats: Different Short- and Long-Term Post-Instillation Results. *Toxicology 264* (1−2), 110−118.

(14) Duffin, R., Tran, L., Brown, D., Stone, V., and Donaldson, K. (2007) Proinflammogenic Effects of Low-Toxicity and Metal Nanoparticles In Vivo and In Vitro: Highlighting the Role of Particle Surface Area and Surface Reactivity. *Inhalation Toxicol. 19* (10), 849−856.

(15) Kennaway, E. L., and Kennaway, N. M. (1947) A Further Study of the Incidence of Cancer of the Lung and Larynx. *Br. J. Cancer 1* (3), 260−298.

(16) Moulin, J. J., Clavel, T., Roy, D., Dananche, B., Marquis, N., Fevotte, J., and Fontana, J. M. (2000) Risk of Lung Cancer in Workers Producing Stainless Steel and Metallic Alloys. *Int. Arch. Occup. Environ. Health 73* (3), 171−180.

(17) Faulds, J. S., and Stewart, M. J. (1956) Carcinoma of the Lung in Hæmatite Miners. *J. Pathol. Bacteriol. 72* (2), 353−366.

(18) Bourgkard, E., Wild, P., Courcot, B., Diss, M., Ettlinger, J., Goutet, P., Hemon, D., Marquis, N., Mur, J. M., Rigal, C., et al. (2009) Lung Cancer Mortality and Iron Oxide Exposure in a French Steel-Producing Factory. *Occup. Environ. Med. 66* (3), 175−181.

(19) Teculescu, D., and Albu, A. (1973) Pulmonary Function in Workers Inhaling Iron Oxide Dust. *Int. Arch. Occup. Environ. Health 31* (2), 163−170.

(20) Turner, H. M., and Grace, H. G. (1938) An Investigation into Cancer Mortality among Males in Certain Sheffield Trades. *J. Hyg. 38* (1), 90−103.

(21) Boyd, J. T., Doll, R., Faulds, J. S., and Leiper, J. (1970) Cancer of the Lung in Iron Ore (Haematite) Miners. *Occup. Environ. Med. 27* (2), 97−105.

(22) Siew, S. S., Kauppinen, T., Kyyronen, P., Heikkila, P., and Pukkala, E. (2008) Exposure to Iron and Welding Fumes and the Risk of Lung Cancer. *Scand. J. Work, Environ. Health 34* (6), 444−450.

(23) Chen, S. Y., Hayes, R. B., Liang, S. R., Li, Q. G., Stewart, P. A., and Blair, A. (1990) Mortality Experience of Haematite Mine Workers in China. *Occup. Environ. Med. 47* (3), 175−181.

(24) Pelclova, D., Zdimal, V., Kacer, P., Fenclova, Z., Vlckova, S., Syslova, K., Navratil, T., Schwarz, J., Zikova, N., Barosova, H., Turci, F., Komarc, M., Pelcl, T., Belacek, J., Kukutschova, J., Zakharov, S.,

DOI: 10.1021/acs.chemrestox.9b00118
Chem. Res. Toxicol. 2019, 32, 2382−2397

et al. (2016) Oxidative Stress Markers Are Elevated in Exhaled Breath Condensate of Workers Exposed to Nanoparticles during Iron Oxide Pigment Production. *J. Breath Res. 10* (1), 016004.
(25) Xing, M., Zhang, Y., Zou, H., Quan, C., Chang, B., Tang, S., and Zhang, M. (2015) Exposure Characteristics of Ferric Oxide Nanoparticles Released during Activities for Manufacturing Ferric Oxide Nanomaterials. *Inhalation Toxicol. 27* (3), 138−148.
(26) Coricovac, D.-E., Moaca, E.-A., Pinzaru, I., Cîtu, C., Soica, C., Mihali, C.-V., Pacurariu, C., Tutelyan, V. A., Tsatsakis, A., and Dehelean, C.-A. (2017) Biocompatible Colloidal Suspensions Based on Magnetic Iron Oxide Nanoparticles: Synthesis, Characterization and Toxicological Profile. *Front. Pharmacol. 8*, 154.
(27) Freyria, F. S., Bonelli, B., Tomatis, M., Ghiazza, M., Gazzano, E., Ghigo, D., Garrone, E., and Fubini, B. (2012) Hematite Nanoparticles Larger than 90 Nm Show No Sign of Toxicity in Terms of Lactate Dehydrogenase Release, Nitric Oxide Generation, Apoptosis, and Comet Assay in Murine Alveolar Macrophages and Human Lung Epithelial Cells. *Chem. Res. Toxicol. 25* (4), 850−861.
(28) Karlsson, H. L., Gustafsson, J., Cronholm, P., and Moller, L. (2009) Size-Dependent Toxicity of Metal Oxide Particles–a Comparison between Nano- and Micrometer Size. *Toxicol. Lett. 188* (2), 112−118.
(29) Totsuka, Y., Ishino, K., Kato, T., Goto, S., Tada, Y., Nakae, D., Watanabe, M., and Wakabayashi, K. (2014) Magnetite Nanoparticles Induce Genotoxicity in the Lungs of Mice via Inflammatory Response. *Nanomaterials 4* (1), 175−188.
(30) Ishino, K., Kato, T., Kato, M., Shibata, T., Watanabe, M., Wakabayashi, K., Nakagama, H., and Totsuka, Y. (2015) Comprehensive DNA Adduct Analysis Reveals Pulmonary Inflammatory Response Contributes to Genotoxic Action of Magnetite Nanoparticles. *Int. J. Mol. Sci. 16* (2), 3474−3492.
(31) Bhattacharya, K., Davoren, M., Boertz, J., Schins, R. P., Hoffmann, E., and Dopp, E. (2009) Titanium Dioxide Nanoparticles Induce Oxidative Stress and DNA-Adduct Formation but Not DNA-Breakage in Human Lung Cells. *Part. Fibre Toxicol. 6*, 17.
(32) Watson, C., Ge, J., Cohen, J., Pyrgiotakis, G., Engelward, B. P., and Demokritou, P. (2014) High-Throughput Screening Platform for Engineered Nanoparticle-Mediated Genotoxicity Using CometChip Technology. *ACS Nano 8* (3), 2118−2133.
(33) Sighinolfi, G. L., Artoni, E., Gatti, A. M., and Corsi, L. (2014) Carcinogenic Potential of Metal Nanoparticles in BALB/3T3 Cell Transformation Assay. *Environ. Toxicol. 31* (5), 509−519.
(34) Stueckle, T. A., Davidson, D. C., Derk, R., Kornberg, T. G., Schwegler-Berry, D., Pirela, S. V., Deloid, G., Demokritou, P., Luanpitpong, S., Rojanasakul, Y., and Wang, L. (2017) Evaluation on Carcinogenesis Potential of Fe2O3 and CeO2 Nanoparticles by a Rapid in Vitro Screening Model. *NanoImpact 6* (1), 39.
(35) Zeidler-Erdely, P. C., Salmen, R., Erdely, A., Keane, M., Kodali, V., Antonini, F., and Falcone, L. (2017) Pulmonary Toxicity of Gas Metal Arc-Stainless Steel Welding Fume and Component Metals. *Toxicol. 150* (1), 2125.
(36) Falcone, L. M., Erdely, A., Kodali, V., Salmen, R., Battelli, L. A., Dodd, T., McKinney, W., Stone, S., Donlin, M., Leonard, H. D., et al. (2018) Inhalation of Iron-Abundant Gas Metal Arc Welding-Mild Steel Fume Promotes Lung Tumors in Mice. *Toxicology 409*, 24−32.
(37) Liu, Y., Li, J., Xu, K., Gu, J., Huang, L., Zhang, L., Liu, N., Kong, J., Xing, M., Zhang, L., et al. (2018) Characterization of Superparamagnetic Iron Oxide Nanoparticle-Induced Apoptosis in PC12 Cells and Mouse Hippocampus and Striatum. *Toxicol. Lett. 292*, 151−161.
(38) Guha, N., Loomis, D., Guyton, K. Z., Grosse, Y., El Ghissassi, F., Bouvard, V., Benbrahim-Tallaa, L., Vilahur, N., Muller, K., Straif, K., et al. (2017) Carcinogenicity of Welding, Molybdenum Trioxide, and Indium Tin Oxide. *Lancet Oncol. 18* (5), 581−582.
(39) Andujar, P., Simon-Deckers, A., Galateau-Sallé, F., Fayard, B., Beaune, G., Clin, B., Billon-Galland, M.-A., Durupthy, O., Pairon, J.-C., Doucet, J., et al. (2014) Role of Metal Oxide Nanoparticles in Histopathological Changes Observed in the Lung of Welders. *Part. Fibre Toxicol. 11*, 23.
(40) Xiong, W., Wang, L., and Yu, F. (2014) Regulation of Cellular Iron Metabolism and Its Implications in Lung Cancer Progression. *Med. Oncol. 31* (7), 28.
(41) Gass, S., Cohen, J. M., Pyrgiotakis, G., Sotiriou, G. A., Pratsinis, S. E., and Demokritou, P. (2013) A Safer Formulation Concept for Flame-Generated Engineered Nanomaterials. *ACS Sustainable Chem. Eng. 1* (7), 843−857.
(42) Sotiriou, G. A., Watson, C., Murdaugh, K. M., Darrah, T. H., Pyrgiotakis, G., Elder, A., Brain, J. D., and Demokritou, P. (2014) Engineering Safer-by-Design Silica-Coated ZnO Nanorods with Reduced DNA Damage Potential. *Environ. Sci.: Nano 1*, 144.
(43) Antonini, J. M., Lawryk, N. J., Murthy, G. G., and Brain, J. D. (1999) Effect of Welding Fume Solubility on Lung Macrophage Viability and Function in Vitro. *J. Toxicol. Environ. Health, Part A 58* (6), 343−363.
(44) Sager, T. M., Porter, D. W., Robinson, V. A., Lindsley, W. G., Schwegler-Berry, D. E., and Castranova, V. (2007) Improved Method to Disperse Nanoparticles for in Vitro and in Vivo Investigation of Toxicity. *Nanotoxicology 1* (2), 118−129.
(45) Hackley, V. A., and Stefaniak, A. B. (2013) Real-World" precision, Bias, and between-Laboratory Variation for Surface Area Measurement of a Titanium Dioxide Nanomaterial in Powder Form. *J. Nanopart. Res. 15* (6), 1.
(46) Cohen, J. M., Beltran-Huarac, J., Pyrgiotakis, G., and Demokritou, P. (2018) Effective Delivery of Sonication Energy to Fast Settling and Agglomerating Nanomaterial Suspensions for Cellular Studies: Implications for Stability, Particle Kinetics, Dosimetry and Toxicity. *NanoImpact 10*, 81−86.
(47) Deloid, G. M., Cohen, J. M., Pyrgiotakis, G., and Demokritou, P. (2017) Preparation, Characterization, and in Vitro Dosimetry of Dispersed, Engineered Nanomaterials. *Nat. Protoc. 12* (2), 355−371.
(48) Cohen, J., DeLoid, G., Pyrgiotakis, G., and Demokritou, P. (2013) Interactions of Engineered Nanomaterials in Physiological Media and Implications for *in Vitro* Dosimetry. *Nanotoxicology 7* (4), 417−431.
(49) Stefaniak, A. B., Guilmette, R. A., Day, G. A., Hoover, M. D., Breysse, P. N., and Scripsick, R. C. (2005) Characterization of Phagolysosomal Simulant Fluid for Study of Beryllium Aerosol Particle Dissolution. *Toxicol. In Vitro 19* (1), 123−134.
(50) DeLoid, G., Cohen, J. M., Darrah, T., Derk, R., Rojanasakul, L., Pyrgiotakis, G., Wohlleben, W., and Demokritou, P. (2014) Estimating the Effective Density of Engineered Nanomaterials for in Vitro Dosimetry. *Nat. Commun. 5*, 3514.
(51) Cohen, J. M., Teeguarden, J. G., and Demokritou, P. (2014) An Integrated Approach for the in Vitro Dosimetry of Engineered Nanomaterials. *Part. Fibre Toxicol. 11* (1), 20.
(52) DeLoid, G. M., Cohen, J. M., Pyrgiotakis, G., Pirela, S. V., Pal, A., Liu, J., Srebric, J., and Demokritou, P. (2015) Advanced Computational Modeling for in Vitro Nanomaterial Dosimetry. *Part. Fibre Toxicol. 12*, 32.
(53) Teeguarden, J. G, Mikheev, V. B, Minard, K. R, Forsythe, W. C, Wang, W., Sharma, G., Karin, N., Tilton, S. C, Waters, K. M, Asgharian, B., Price, O. R, Pounds, J. G, and Thrall, B. D (2014) Comparative Iron Oxide Nanoparticle Cellular Dosimetry and Response in Mice by the Inhalation and Liquid Cell Culture Exposure Routes. *Part. Fibre Toxicol. 11*, 46.
(54) Chen, B. T., Schwegler-Berry, D., Cumpston, A., Cumpston, J., Friend, S., Stone, S., and Keane, M. (2016) Performance of a Scanning Mobility Particle Sizer in Measuring Diverse Types of Airborne Nanoparticles: Multi-Walled Carbon Nanotubes, Welding Fumes, and Titanium Dioxide Spray. *J. Occup. Environ. Hyg. 13* (7), 501−518.
(55) Espósito, B. P., Epsztejn, S., Breuer, W., and Cabantchik, Z. I. (2002) A Review of Fluorescence Methods for Assessing Labile Iron in Cells and Biological Fluids. *Anal. Biochem. 304* (1), 1−18.
(56) Buss, J. L., Arduini, E., and Ponka, P. (2002) Mobilization of Intracellular Iron by Analogs of Pyridoxal Isonicotinoyl Hydrazone (PIH) Is Determined by the Membrane Permeability of the Iron-Chelator Complexes. *Biochem. Pharmacol. 64* (12), 1689−1701.

DOI: 10.1021/acs.chemrestox.9b00118
Chem. Res. Toxicol. 2019, 32, 2382−2397

(57) Hanahan, D., and Weinberg, R. A. (2011) Hallmarks of Cancer: The Next Generation. *Cell 144* (5), 646−674.
(58) Horibata, S., Vo, T. V., Subramanian, V., Thompson, P. R., and Coonrod, S. A. (2015) Utilization of the Soft Agar Colony Formation Assay to Identify Inhibitors of Tumorigenicity in Breast Cancer Cells. *J. Visualized Exp.* No. 99, No. e52727.
(59) O'Connor, M. J. (2015) Targeting the DNA Damage Response in Cancer. *Mol. Cell 60* (4), 547−560.
(60) Lorat, Y., Timm, S., Jakob, B., Taucher-Scholz, G., and Rübe, C. E. (2016) Clustered Double-Strand Breaks in Heterochromatin Perturb DNA Repair after High Linear Energy Transfer Irradiation. *Radiother. Oncol. 121* (1), 154−161.
(61) Nikitaki, Z., Nikolov, V., Mavragani, I. V., Mladenov, E., Mangelis, A., Laskaratou, D. A., Fragkoulis, G. I., Hellweg, C. E., Martin, O. A., Emfietzoglou, D., et al. (2016) Measurement of Complex DNA Damage Induction and Repair in Human Cellular Systems after Exposure to Ionizing Radiations of Varying Linear Energy Transfer (LET). *Free Radical Res. 50*, S64−S78.
(62) Evans, M. D., Dizdaroglu, M., and Cooke, M. S. (2004) Oxidative DNA Damage and Disease: Induction, Repair and Significance. *Mutat. Res., Rev. Mutat. Res. 567* (1), 1−61.
(63) Stueckle, T. A., Davidson, D. C., Derk, R., Demokritou, P., Kornberg, T., Schwegler-Berry, D., and Wang, L. (2016) Nano-Ferric Oxide Induced Neoplastic-Like Transformation in a Human Primary Cell Model: Iron Homeostasis Disruption? *Toxicol. 2783*, 419.
(64) Villeneuve, P. J., Jerrett, M., Brenner, D., Su, J., Chen, H., and McLaughlin, J. R. (2014) A Case-Control Study of Long-Term Exposure to Ambient Volatile Organic Compounds and Lung Cancer in Toronto, Ontario, Canada. *Am. J. Epidemiol. 179* (4), 443−451.
(65) Hanahan, D., and Weinberg, R. A. (2000) The Hallmarks of Cancer. *Cell 100* (1), 57−70.
(66) Wang, Y., Cui, H., Zhou, J., Li, F., Wang, J., Chen, M., and Liu, Q. (2015) Cytotoxicity, DNA Damage, and Apoptosis Induced by Titanium Dioxide Nanoparticles in Human Non-Small Cell Lung Cancer A549 Cells. *Environ. Sci. Pollut. Res. 22* (7), 5519−5530.
(67) Setyawati, M. I., Sevencan, C., Bay, B. H., Xie, J., Zhang, Y., Demokritou, P., and Leong, D. T. (2018) Nano-TiO2Drives Epithelial-Mesenchymal Transition in Intestinal Epithelial Cancer Cells. *Small 14* (30), 1800922.
(68) Hong, F., Ji, L., Zhou, Y., and Wang, L. (2017) Chronic Nasal Exposure to Nanoparticulate TiO_2 Causes Pulmonary Tumorigenesis in Male Mice. *Environ. Toxicol. 32* (5), 1651−1657.
(69) Donaldson, K., Schinwald, A., Murphy, F., Cho, W. S., Duffin, R., Tran, L., and Poland, C. (2013) The Biologically Effective Dose in Inhalation Nanotoxicology. *Acc. Chem. Res. 46* (3), 723−732.
(70) Galaris, D., and Pantopoulos, K. (2008) Oxidative Stress and Iron Homeostasis: Mechanistic and Health Aspects. *Crit. Rev. Clin. Lab. Sci. 45* (1), 1−23.
(71) Tenopoulou, M., Doulias, P. T., Barbouti, A., Brunk, U., and Galaris, D. (2005) Role of Compartmentalized Redox-Active Iron in Hydrogen Peroxide-Induced DNA Damage and Apoptosis. *Biochem. J. 387* (3), 703−710.
(72) Mesárošová, M., Kozics, K., Bábelová, A., Regendová, E., Pastorek, M., Vnuková, D., Buliaková, B., Rázga, F., and Gábelová, A. (2014) The Role of Reactive Oxygen Species in the Genotoxicity of Surface-Modified Magnetite Nanoparticles. *Toxicol. Lett. 226* (3), 303−313.
(73) Kamiyama, T., Miyakawa, H., Li, J. P., Liu, J., Liu, J. H., Marumo, F., Sato, C., and Akiba, T. (1995) Effects of One-Year Cadmium Exposure on Livers and Kidneys and Their Relation to Glutathione Levels. *Res. Commun. Mol. Pathol. Pharmacol. 88* (2), 177−186.
(74) Prozialeck, W. C., Vaidya, V. S., Liu, J., Waalkes, M. P., Edwards, J. R., Lamar, P. C., Bernard, A. M., Dumont, X., and Bonventre, J. V. (2007) Kidney Injury Molecule-1 Is an Early Biomarker of Cadmium Nephrotoxicity. *Kidney Int. 72* (8), 985.
(75) Liu, J., Qu, W., and Kadiiska, M. B. (2009) Role of Oxidative Stress in Cadmium Toxicity and Carcinogenesis. *Toxicol. Appl. Pharmacol. 238* (3), 209−214.
(76) Chang, Q., Pan, J., Wang, X., Zhang, Z., Chen, F., and Shi, X. (2010) Reduced Reactive Oxygen Species-Generating Capacity Contributes to the Enhanced Cell Growth of Arsenic-Transformed Epithelial Cells. *Cancer Res. 70* (12), 5127−5135.
(77) Shoeb, M., Kodali, V., Farris, B., Bishop, L. M., Meighan, T., Salmen, R., Eye, T., Roberts, J. R., Zeidler-Erdely, P., Erdely, A., et al. (2017) Evaluation of the Molecular Mechanisms Associated with Cytotoxicity and Inflammation after Pulmonary Exposure to Different Metal-Rich Welding Particles. *Nanotoxicology 11* (6), 1−12.
(78) Lu, X., Miousse, I. R., Pirela, S. V., Melnyk, S., Koturbash, I., and Demokritou, P. (2016) Short-Term Exposure to Engineered Nanomaterials Affects Cellular Epigenome. *Nanotoxicology 10* (2), 1−11.
(79) Zhang, T., Qi, Y., Liao, M., Xu, M., Bower, K. A., Frank, J. A., Shen, H. M., Luo, J., Shi, X., and Chen, G. (2012) Autophagy Is a Cell Self-Protective Mechanism against Arsenic-Induced Cell Transformation. *Toxicol. Sci. 130* (2), 298−308.
(80) Gupta, A. K., Naregalkar, R. R., Vaidya, V. D., and Gupta, M. (2007) Recent Advances on Surface Engineering of Magnetic Iron Oxide Nanoparticles and Their Biomedical Applications. *Nanomedicine (London, U. K.) 2* (1), 23−39.
(81) Bekaroglu, M. G., İşçi, Y., and İşçi, S. (2017) Colloidal Properties and in Vitro Evaluation of Hydroxy Ethyl Cellulose Coated Iron Oxide Particles for Targeted Drug Delivery. *Mater. Sci. Eng., C 78*, 847−853.
(82) Truzzi, E., Bongio, C., Sacchetti, F., Maretti, E., Montanari, M., Iannuccelli, V., Vismara, E., and Leo, E. (2017) Self-Assembled Lipid Nanoparticles for Oral Delivery of Heparin-Coated Iron Oxide Nanoparticles for Theranostic Purposes. *Molecules 22* (6), 963.
(83) Ma, J., Mercer, R. R., Barger, M., Schwegler-Berry, D., Cohen, J. M., Demokritou, P., and Castranova, V. (2015) Effects of Amorphous Silica Coating on Cerium Oxide Nanoparticles Induced Pulmonary Responses. *Toxicol. Appl. Pharmacol. 288* (1), 63−73.
(84) McKeon, K. D., and Love, B. J. (2008) The Presence of Adsorbed Proteins on Particles Increases Aggregated Particle Sedimentation, as Measured by a Light Scattering Technique. *J. Adhes. 84* (7), 664−674.
(85) Davidson, D. C., Derk, R., He, X., Stueckle, T. A., Cohen, J., Pirela, S. V., Demokritou, P., Rojanasakul, Y., and Wang, L. (2015) Direct Stimulation of Human Fibroblasts by nCeO2 in Vitro Is Attenuated with an Amorphous Silica Coating. *Part. Fibre Toxicol. 13* (1), 23.
(86) Ma, J. Y., Zhao, H., Mercer, R. R., Barger, M., Rao, M., Meighan, T., Schwegler-Berry, D., Castranova, V., and Ma, J. K. (2011) Cerium Oxide Nanoparticle-Induced Pulmonary Inflammation and Alveolar Macrophage Functional Change in Rats. *Nanotoxicology 5* (3), 312−325.
(87) Konduru, N. V., Jimenez, R. J., Swami, A., Friend, S., Castranova, V., Demokritou, P., Brain, J. D., and Molina, R. M. (2015) Silica Coating Influences the Corona and Biokinetics of Cerium Oxide Nanoparticles. *Part. Fibre Toxicol. 12* (1), 1.
(88) Konduru, N. V., Murdaugh, K. M., Sotiriou, G. A., Donaghey, T. C., Demokritou, P., Brain, J. D., and Molina, R. M. (2014) Bioavailability, Distribution and Clearance of Tracheally-Instilled and Gavaged Uncoated or Silica-Coated Zinc Oxide Nanoparticles. *Part. Fibre Toxicol. 11* (1), 1.
(89) Demokritou, P., Gass, S., Pyrgiotakis, G., Cohen, J. M., Goldsmith, W., McKinney, W., Frazer, D., Ma, J., Schwegler-Berry, D., Brain, J., et al. (2013) An in Vivo and in Vitro Toxicological Characterisation of Realistic Nanoscale CeO2 Inhalation Exposures. *Nanotoxicology 7* (8), 1338−1350.

DOI: 10.1021/acs.chemrestox.9b00118
Chem. Res. Toxicol. 2019, 32, 2382−2397